photonics

MDPI

Review

Technological Evolution in Grating Encoders: A Review

Yikai Zhang †, Bing Xie †, Yuliang Ye, Kangcheng Wu and Xin Xiong *

Engineering Research Center of Mechanical Testing Technology and Equipment (Ministry of Education), Chongqing University of Technology, Chongqing 400054, China; yikaizhang@stu.cqut.edu.cn (Y.Z.); bingxie@stu.cqut.edu.cn (B.X.)

* Correspondence: xinxiong@cqut.edu.cn

† These authors contributed equally to this work.

Abstract

As core components for ultra-precision positioning, grating encoders have technologically evolved toward higher accuracy, faster speeds, and multi-degree-of-freedom (multi-DOF) integration. This review systematically traces the technological progression of commercial grating encoders from imaging scanning to interferential scanning, from incremental to absolute encoding, and from single axis to multi-DOF integration. It compares the distinct technical strategies adopted by Heidenhain and Renishaw for robustness enhancement and absolute encoding within the imaging scanning paradigm. It also uncovers the physical mechanism of optical subdivision that allows interferential scanning encoders to surpass the sub-nanometer resolution barrier. Building upon this foundation, recent academic advances in multi-DOF interferometric measurement systems and Fizeau interferometer-based grating self-calibration methodologies are also reviewed.

Keywords: grating encoders; imaging scanning; interferential scanning; incremental; absolute; multi-DOF measurement; self-calibration

1. Introduction

In strategic fields including ultra-precision manufacturing, semiconductor equipment, optical system integration, and high-end scientific instrumentation, system performance is steadily approaching the sub-nanometer and even picometer frontiers of positioning accuracy [1,2]. As the cornerstone of precision motion control [3], displacement measurement directly dictates the levels of machining precision, alignment integrity, and measurement reliability achievable. Hence, advancing displacement sensing technologies with high resolution, robust stability, and multi-DOF capability [4,5] has emerged as a central mission for propelling technological progress across these fields.

High-precision displacement sensors currently available [6–9] fall roughly into two main classes according to their working principles: electrical and optical. Electrical-type sensors primarily encompass inductive, eddy-current, and capacitive varieties. Among these, eddy-current sensors offer a measurement range of up to millimeters while attaining micrometer-level precision [10–13]; capacitive displacement sensors, by comparison, achieve nanometer precision under single-degree-of-freedom conditions, albeit with a linear measurement range generally confined to several hundred micrometers [14,15]. Moreover, when employed for three-degree-of-freedom measurements, capacitive displacement sensors see their accuracy drop to the micrometer scale [16]. On the whole, electrical-type sensors provide good resolution and dynamic response over certain ranges, rendering

Check for updates

Received: 18 June 2026
Revised: 26 July 2026
Accepted: 27 July 2026
Published: 31 July 2026

Copyright: © 2026 by the authors. Licensee MDPI, Basel, Switzerland. This article is an open access article distributed under the terms and conditions of the Creative Commons Attribution (CC BY) license.

them especially suitable for complex environments demanding high immunity to interference. However, they remain constrained in measurement range, long-term stability, and environmental robustness.

Optical displacement sensors, especially laser interferometers and grating encoders, have by contrast emerged as the dominant technological route for ultra-precision displacement measurement, owing to their non-contact operation, high resolution, and rapid response. Of these, laser interferometers adopt the laser wavelength as their metrological reference [17,18]. Given that laser interferometers generally involve long optical paths, their measurement performance is vulnerable to variations in air refractive index, which induce wavelength instability [19] and consequently restrict their use in non-conditioned environments [20–22]. Grating encoders, by contrast, rely on the physical grating pitch as their metrological reference and harness the diffraction effect of gratings, thereby facilitating single-point multi-degree-of-freedom displacement measurement with inherently greater structural stability [23]. The measurement accuracy of grating encoders is determined primarily by the precision and uniformity of the grating pitch [24–27]. Grating encoders are capable of both nanoscale absolute displacement measurement [28,29] and, under optical arrangements, angular measurement [30,31]. Consequently, in domains such as semiconductor manufacturing equipment, ultra-precision machine tools, and robotics—where positioning accuracy and system reliability are paramount—grating encoders have become among the most widely adopted displacement sensing components [32].

In terms of system architecture, a grating encoder is generally composed of three elements: the grating that acts as the metrological reference, an optical reading head that acquires grating signals, and an interpolation circuit that electronically subdivides and processes the reading head output signals [33]. Based on the output signal format, grating encoders fall into two categories: incremental and absolute [34]. An incremental encoder represents position information through equally spaced grating marks and measures relative displacement by counting the marks traversed from a starting reference point. In principle, this encoding scheme places no constraint on the scale length. An absolute encoder, by contrast, assigns a fixed-bit code to each mark, enabling direct readout of absolute position. While the measurement range of an absolute encoder is constrained by its code bit length, it provides benefits including low miscount risk, high immunity to interference, power-on readiness, and retained position after power loss. These features render it more efficient and safer than incremental encoders, which demand a reference return (homing) operation.

Additionally, based on the photoelectric scanning principle, grating encoders fall into two categories: imaging scanning and interference scanning. Imaging scanning encoders generally employ gratings with a 20 μm pitch, whereas interference scanning encoders are suited for a grating pitch of 8 μm. Interference scanning encoders, operating on the principle of diffractive interference, can attain extreme resolution and accuracy down to the sub-nanometer and even picometer scale [35].

This review examines the technological evolution and performance breakthroughs of grating encoders, mostly those that are commercially available across three dimensions: measurement principles, encoding methodologies, and multi-DOF integration. First, imaging scanning encoders are addressed, with an analysis of their Moiré fringe signal generation mechanism, followed by a comparison of the distinct technical strategies adopted by Heidenhain and Renishaw for robustness enhancement and absolute encoding realization. Second, interferential scanning encoders are examined, illustrating how the principle of diffractive interference overcomes resolution limitations through optical subdivision. Using Heidenhain's LIP series and Sony Magnescale as case studies, the technological basis for picometer-scale metrology is disclosed. The discussion then expands to multi-DOF

measurement systems, reviewing interferometric approaches for two-dimensional planar, three-dimensional spatial, and six-DOF pose detection. Building on this foundation, the current frontier research directions and technical challenges in grating-based displacement metrology are further identified. Through the foregoing analysis, this review is intended to offer a systematic theoretical reference for the selection, application, and technological innovation of grating encoders.

Figure 1 presents the overall framework of grating encoders covered in this review, organized from the viewpoints of technical classification and system integration. Based on the photoelectric scanning principle, grating encoders fall into two broad categories: imaging scanning and interferential scanning, which correspond to the main topics of Sections 2 and 3, respectively. By signal output type, they are further categorized as incremental and absolute encoders, whose critical technological advances are highlighted in Sections 2.3 and 3.1, respectively. In addition, the figure incorporates multi-DOF encoders and grating metrology techniques, which will form the core of Section 4 (Multi-DOF Grating Interferometer Measurement Systems) and Section 5 (Diffraction Grating Self-Calibration). The following chapters will be developed systematically in accordance with this framework.

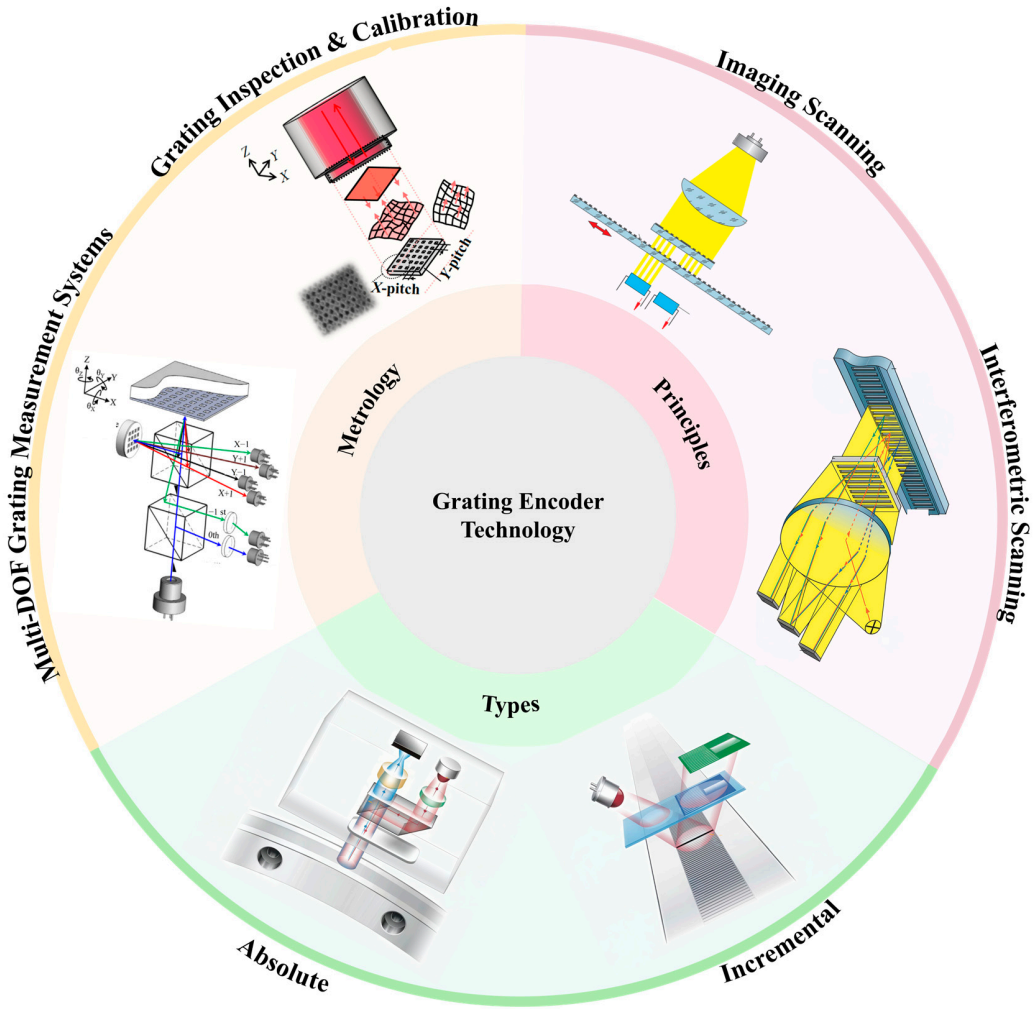


Figure 1. Technical classification, system integration, and structural overview of grating encoders covered in this review.

2. Imaging Scanning Grating Encoders

Optical imaging scanning encoders realize precision displacement measurement mainly by controlling light intensity, employing either a single grating together with

a scanning mask or two gratings—namely, a scale grating and an index grating. In incremental configurations, the scale grating typically features only a single track of periodic lines. In absolute configurations, an additional coded track is usually present; both tracks are illuminated at the same time, and displacement is retrieved from the measured intensity distribution pattern of the returning light. The core principle involves encoding measurement based on light intensity patterns, with coding formats such as maximum-length sequence (M-sequence) codes and Gray codes being widely adopted.

2.1. Moiré Fringe Imaging Scanning Principle

Imaging scanning techniques rely on geometric projection of gratings and the Moiré fringe effect [36–39], and are applicable to grating pitches of 20 μm and above. As illustrated in Figure 2a, the fundamental principle involves modulation of transmitted light [40,41]. A scanning mask (typically consisting of opaque grating lines on a transparent substrate) and a scale grating (which may be transmissive or reflective) having an identical or closely matched pitch undergo relative motion with respect to each other. When collimated light passes through or reflects from the scale grating, alternating bright and dark projected fringes are generated at a particular plane, and the scanning mask is positioned precisely within this plane. As the two gratings move relative to one another, light transmits through regions where the slits are aligned and is blocked where they are misaligned, thus producing intensity modulation of the incoming light. A photodetector array transduces the intensity variations into electrical signals. The distinctive grating pattern of the scanning mask shapes the light intensity modulation into an approximately sinusoidal output signal. As the grating pitch decreases, the required separation between the scanning mask and the scale grating diminishes, and the associated tolerances become more stringent. A representative enclosed imaging-scanning encoder structure integrating the light source, scale grating, index grating, and readout components is shown in Figure 2d [42].

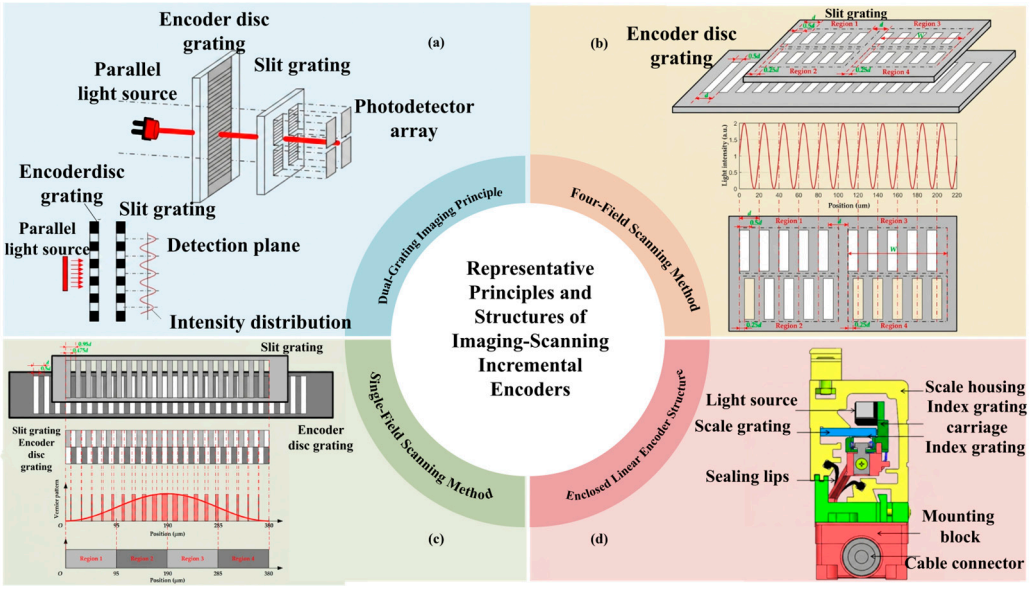


Figure 2. Representative principles and structures of imaging-scanning encoders: (**a**) dual-grating imaging principle; (**b**) four-field scanning method; (**c**) single-field scanning method; and (**d**) enclosed image-scanning linear encoder structure. Panels (**a**–**c**) were adapted from Ref. [41], and panel (**d**) was adapted from Ref. [42].

2.2. Comparative Analysis of Anti-Interference Techniques for Incremental Schemes

Imaging scanning incremental encoders measure relative position by counting the grating marks traversed from a reference mark. The precision and robustness of such

encoders are mainly constrained by three factors: signal attenuation from grating surface contamination, higher-order harmonic distortion within the Moiré fringe signals, and amplitude fluctuations induced by mounting tolerances. To overcome these challenges, various manufacturers have pursued differentiated technological strategies. Notably, Heidenhain's single-field scanning and Renishaw's spatial filtering plus multi-fringe averaging stand out as the most representative approaches.

2.2.1. Advancement of Single-Field Scanning Technology

In the domain of grating-based displacement measurement, Heidenhain's enclosed linear encoders, including the LC, LS, and LB series, utilize well-established optical imaging scanning techniques. Within the imaging scanning paradigm, Heidenhain's product portfolio has evolved technologically from four-field scanning to single-field scanning, with the distinction lying in the design of the scanning mask and the corresponding signal generation architecture.

Four-field scanning represents an early classical approach [41]. As illustrated in Figure 2b, the scanning mask is partitioned into four independent fields mutually separated by a 90° phase shift, each paired with a photodiode, yielding four raw output signals. Owing to the presence of direct-current (DC) offsets and vulnerability to contamination, differential processing becomes necessary to derive quadrature sinusoidal and cosinusoidal signals. This configuration is highly sensitive to localized grating contamination and exhibits elevated harmonic content, thereby constraining the efficacy of optical filtering.

To address the aforementioned limitations, Heidenhain introduced single-field scanning technology [41], illustrated in Figure 2c, featuring a mask with a dissimilar grating pitch and a large-area photodetector array. The pairing of mismatched grating pitches induces an optical beating effect, which efficiently attenuates higher-order harmonics and directly yields a clean sinusoidal intensity distribution. The detector array spatially samples the entire intensity field and synthesizes quadrature signals, rendering the system highly robust to localized contamination and installation tolerances. Comparing Figure 2b and Figure 2c, single-field scanning substitutes the conventional four-field discrete architecture with a structured mask design and array-based detection, thereby fundamentally enhancing signal quality and immunity to disturbances.

2.2.2. Spatial Filtering and Multiple-Fringe Averaging Technology

Renishaw has advanced robustness-enhancing techniques grounded in spatial filtering. The company's RG and TONiC encoder series incorporate an optical system featuring an integrated filtering grating [43]. In this approach, a pitch-matched index grating is introduced into the optical path. It spatially filters the diffracted light returning from the scale grating, regenerates pristine interference fringes, and subsequently images these fringes onto the photodetector. This spatial filtering mechanism ensures stable quadrature signal output from the detector even in the presence of localized contamination on the scale grating surface.

To mitigate the effects of grating scale errors, the system adopts multi-fringe imaging combined with signal averaging. The photodetector array simultaneously acquires intensity data spanning tens to hundreds of grating periods; a digital signal processor (DSP) then performs real-time averaging to smooth out local irregularities, thereby enhancing the overall system precision. This design simultaneously relaxes mounting tolerances by accommodating moderate pitch and yaw misalignments, thus improving practical engineering adaptability.

To summarize, Heidenhain's single-field scanning technology minimizes harmonic content and susceptibility to contamination via a mismatched-pitch mask and full-field

sampling, while Renishaw achieves robustness through spatial filtering gratings combined with multi-fringe averaging. Although the two approaches diverge considerably in their engineering realization, both have proven effective in enhancing the contamination immunity and signal fidelity of imaging scanning encoders.

2.3. Absolute Encoders

2.3.1. High Velocity and High Resolution Absolute Encoders

Beyond the ever-increasing requirements for measurement precision, the demand for high-speed measurement capability is also steadily rising. Absolute encoders likewise possess inherent advantages in addressing the need for high-speed operation. In traditional incremental encoders, the sinusoidal voltage signal from the reading head is subsequently processed by an interpolator that carries out interpolation and further subdivision. The maximum electrically sustainable measurement speed $v_{\max}$ of an encoder is constrained by the carrier frequency f_c of the reading head, given by the following expression [33]:

$$v_{\max} = p \cdot f_c \tag{1}$$

In this expression, p denotes the period of the sinusoidal voltage signal generated by the reading head, which generally corresponds to the pitch of the scale grating. To attain a resolution d from the native physical period p, the raw signal must undergo high-order subdivision. In theory, the relationship between the equivalent signal frequency f_s following subdivision and the measurement speed can be formulated as:

$$f_s = \frac{v_{\max}}{d} \tag{2}$$

Following quadrature (4×) interpolation, the effective pulse period counted by the electronics reduces to p/4, yielding an actual input frequency of:

$$f_s = \frac{1}{4}\frac{p}{d}f_c = \frac{1}{4}\frac{v_{\max}}{d} \tag{3}$$

Consequently, following subdivision, the pulse frequency f_s to be handled by the downstream electronics rises sharply. Given that the downstream circuitry possesses an upper limit on the tolerable pulse frequency f_s, this constraint inversely limits the encoder's maximum achievable measurement speed:

$$v_{\max} = 4d \cdot f_s \tag{4}$$

As evident from the above analysis, incremental encoders face a fundamental trade-off between resolution and speed. To circumvent this limitation, absolute encoders have been developed. Absolute encoders eliminate the need for continuous pulse counting by directly deriving the position value within the reading head via encoding and decoding schemes, thus enabling higher measurement speeds without sacrificing resolution [37]. The following sections take typical solutions from Heidenhain and Renishaw as examples to illustrate the implementation approaches of imaging scanning absolute encoders.

2.3.2. Dual-Track Encoding and Integrated Decoding

Heidenhain's absolute linear encoders, exemplified by the LIC series [44–46], integrate two distinct physical tracks on a single scale. A representative enclosed absolute linear encoder structure is shown in Figure 3a [42]. Through a dedicated scanning and decoding algorithm, they enable the absolute position to be obtained at any moment without requiring a reference mark return (homing) operation. The essence of this approach resides

in the synergistic integration of high-precision interpolation of the incremental track with encoding and decoding of the absolute track. In such dual-track absolute encoders, the absolute scale incorporates an extra parallel track, dedicated to absolute position encoding in addition to the incremental track. Figure 3b illustrates a representative multi-track Gray-code pattern, in which adjacent code words differ by only one bit. Multi-track encoding thus represents Heidenhain's signature approach for realizing high-accuracy absolute measurement.

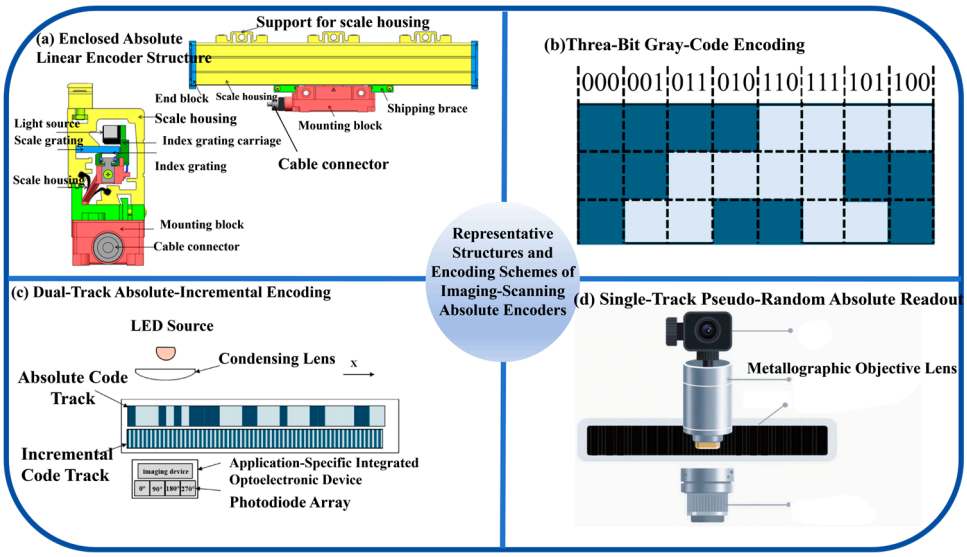


Figure 3. Representative structures and encoding schemes of imaging-scanning absolute encoders: (**a**) enclosed absolute linear-encoder structure; (**b**) multi-track Gray-code encoding; (**c**) dual-track absolute–incremental encoding; and (**d**) single-track pseudo-random absolute readout. Panel (**a**) was adapted from Ref. [42], and panels (**b**–**d**) were adapted from Ref. [37].

The approach exemplified by Heidenhain's LIC series employs a two-track configuration consisting of an incremental track and an absolute track, as illustrated in Figure 3c. The incremental track delivers continuous high-resolution phase information, whereas the absolute track utilizes pseudo-random codes or Gray codes to encode the absolute position. The reading head synchronously scans both tracks. It first decodes the absolute track information to derive a coarse position segment. Subsequently, the sinusoidal voltage signal from the incremental track is digitized by an onboard analog-to-digital converter (ADC), and the internal microprocessor unit (MPU) performs interpolation subdivision on the digital data to yield fine position data at 1 nm resolution. The fine position data is then rapidly fused with the absolute track position data within the MPU, ultimately producing a 1 nm-resolution absolute position value as a numerical output. Since the entire processing chain is carried out numerically within the MPU, this approach avoids the signal distortion inherent in conventional electronic circuits that rely on transmitting high-frequency square-wave voltage signals, thereby demonstrating both high speed and high precision. As no external counter is needed, the instantaneous absolute position value is transmitted only when requested by an external device, at a timing interval compatible with the device's processing cycle, using low-cost serial communication (e.g., RS422). Even with a maximum data transmission frequency of 10 MHz, the communication speed remains adequate for practical needs. Consequently, the maximum measurement speed is governed exclusively by the reading head bandwidth (as expressed in Equation (1)), enabling this system to reach a maximum measurement speed of 10 m/s. Nevertheless, this dual-track configuration imposes stringent mechanical alignment requirements. Notably, its susceptibility to yaw deviations restricts its suitability for certain operational scenarios.

2.3.3. Single-Track Imaging Absolute Positioning

Renishaw's RESOLUTE series absolute optical encoders depart from conventional absolute encoder designs that depend on multiple code tracks or intricate mechanical structures. Instead, they employ a single-track image-based absolute positioning technology [47] founded upon high-speed imaging and real-time image processing. A representative single-track pseudo-random absolute readout configuration is illustrated in Figure 3d. This approach achieves exceptional accuracy and speed while fundamentally addressing issues related to installation tolerances and immunity to contamination.

This technology utilizes single-track pseudo-random encoding, selectively omitting certain scale lines to generate a distinctive "fingerprint" pattern along the grating scale. Within the reading head, a high-speed complementary metal-oxide-semiconductor (CMOS) image sensor is integrated. Upon receipt of a position request, it executes an instantaneous exposure to capture a localized image of the grating. The system further employs a high-speed image sensor (operating at a 1 Gbit/s output data rate) to acquire images of the scale. These image data undergo analog-to-digital conversion at roughly 500 MB/s and are subsequently transferred to a digital signal processor (DSP). Within the DSP, both the high-resolution fine position (within the nominal scale line pitch) and the absolute position of the scale lines are computed from the position code embedded on the scale. These two components are then fused to yield high-resolution absolute position data in numerical form. Subsequently, the resulting absolute position data are transmitted back to the requesting external device through serial communication. The entire cycle receiving a position request to delivering the response takes merely 12 μs and is repeatable at a maximum rate of 25,000 requests per second. Consequently, while preserving a high resolution of 1 nm or 0.01 arcsecond, this system realizes ultra-fast absolute position measurement at linear speeds of up to 100 m/s or rotational speeds as high as 36,000 rpm.

Position determination is achieved through a parallel dual-algorithm architecture. The first algorithm identifies the coarse absolute position via image recognition of the "fingerprint" pattern while simultaneously extracting fringe phase for fine relative positioning. The second algorithm performs linear prediction based on historical position data. The outcomes from both algorithms are mutually validated, guaranteeing exceptional reliability and safety even under high-speed operation and in the presence of contamination. This approach fundamentally removes the yaw sensitivity associated with multi-track encoding and significantly relaxes alignment requirements. The allowable installation tolerances for the reading head with respect to the scale are as follows: $\pm 0.5^{\circ}$ in pitch, yaw, and roll, and 0.8 mm $\pm$ 0.15 mm in the vertical (standoff) direction. Recent studies have also addressed diffraction-aware design and optimization of high-bit zero-position codes for absolute encoders using deep learning approaches [48].

In summary of this section, Table 1 consolidates the key performance specifications of representative imaging-scanning grating encoders from both Heidenhain and Renishaw. As evident from the table, absolute encoders offer substantially higher maximum response speeds compared to traditional incremental counterparts without sacrificing resolution, illustrating the performance gains enabled by advancements in encoding methodologies.

Table 1. Key performance parameters of representative imaging scanning linear encoders from major manufacturers.

Product Models	Manufacturers	Type	Max. Range	Max. Resolution	Max. Speed
LS 400	Heidenhain	Incremental	2040 mm	0.25 μm	2 m/s
LIC 4100	Heidenhain	Absolute	28,000 mm	1 nm	10 m/s
LC 400	Heidenhain	Absolute	670 mm	1 nm	3 m/s

Table 1. *Cont.*

Product Models	Manufacturers	Type	Max. Range	Max. Resolution	Max. Speed
RGH45	Renishaw	Incremental	25,000 mm	0.4 μm	10 m/s
TONiC™	Renishaw	Incremental	20,000 mm	1 nm	10 m/s
RESOLUTE™	Renishaw	Absolute	25,000 mm	1 nm	100 m/s
EVOLUTE™	Renishaw	Absolute	10,020 mm	50 nm	100 m/s

3. Interferential Scanning Grating Encoders

In optical interference scanning encoders [49], when the grating pitch falls below 10 μm, the pitch and the source wavelength approach each other, leading to progressively stronger diffraction. As a rule, a finer grating pitch results in more prominent diffraction behavior. The interference of diffracted light renders the signal period directly traceable to the grating pitch magnitude. When augmented by optical subdivision, the signal period undergoes further reduction, and subsequent electronic subdivision can significantly improve both measurement resolution and accuracy. Moreover, as the grating pitch approaches the source wavelength, the impact of nonlinear interpolation errors can be substantially mitigated. Consequently, nanometer-pitch gratings are particularly favorable for attaining displacement measurement precision at the nanometer or sub-nanometer level [50,51]. Interferential scanning grating measurement systems provide superior resolution and accuracy relative to grating displacement systems based on geometric Moiré fringes, along with greater design flexibility. As a result, they have been more extensively adopted in industrial manufacturing [52].

3.1. Mechanism of Resolution Limit Breakthrough

Resolution is a critical metric for assessing the performance of grating encoders. Within an encoder, the reading head generates two-phase (A/B-phase) sinusoidal voltage signals having a signal period of p from the scale grating. An interpolator subsequently performs electronic subdivision on these signals, converting them into pulse outputs that correspond to the positional resolution. Assuming a total subdivision factor of N, the encoder resolution d is given by [33]:

$$d = p/N \tag{5}$$

where p represents the period of the sinusoidal voltage signal generated by the reading head, which is generally equivalent to the grating pitch m.

According to Equation (5), two approaches are typically adopted to enhance both the resolution and measurement accuracy of grating encoders: decreasing the physical grating pitch or increasing the overall signal subdivision factor [53,54]. However, each approach faces inherent limitations that constrain its practical applicability.

Regarding the approach of reducing the grating pitch: to attain sub-nanometer resolution comparable to laser interferometers, the line spacing must be decreased from the traditional 20 μm scale to the micrometer range, approaching the wavelength of light. Nevertheless, fabrication process constraints make it challenging to preserve grid pattern regularity, thereby compromising grating pitch uniformity [55]. Furthermore, increasing groove density results in substantially higher costs and prolonged manufacturing lead times.

Regarding the approach of increasing the subdivision factor: interpolation techniques encompass both electronic interpolation [56–58] and optical interpolation [59–62]. For electronic interpolation, imperfections inherent in real-world signals, including harmonic distortion, phase errors, and amplitude imbalance, collectively impede the enhancement of

interpolation precision. These deficiencies can lead to signal ambiguity or compromised discrimination within certain intervals when attempting high-factor electronic interpolation. Consequently, the electronic interpolation factor remains constrained, and even with signal compensation techniques, persistent challenges related to operating range and robustness remain.

For enhancing displacement measurement precision, optical interpolation provides greater robustness compared to electronic interpolation. Through the diffraction and interference phenomena of the grating, periodic subdivision is accomplished at the point of signal origination, bringing the +1st and −1st order diffracted beams into interference. For a relative displacement of the grating equal to one physical grating pitch m, the phase of the resultant interference signal shifts by 4π, which indicates that the interference signal undergoes two complete oscillation periods.

Consequently, the effective signal period p is reduced to one half of the physical grating pitch m. By employing more sophisticated optical layouts, optical interpolation factors of 4 or even 16 can be realized [61,62]. This method directly shortens the signal's effective period, independent of electronic circuitry or the inherent limits of grating fabrication, thereby establishing a physical basis for achieving ultra-high resolution.

Moreover, signals produced via the optical division process are characterized by exceptionally high sinusoidal fidelity, with minimal harmonic distortion beyond the fundamental frequency component. This enables stable and reliable ultra-high-factor electronic interpolation of the signal, avoiding the significant errors associated with distortion in traditional signal processing.

Hence, when approaching the upper limit of feasible electronic interpolation, attaining a high degree of optical subdivision via proper optical configuration represents a crucial strategy for improving both the resolution and precision of grating interferometer measurements. This has led to the development and adoption of grating interferometer encoders.

Grounded in the above diffraction interferometry principle, interferential scanning encoders physically realize optical subdivision of the grating period, fundamentally improving both signal integrity and the potential for high resolution. At present, the primary technical routes for implementing this principle are dual-grating interferometry and holographic grating-based self-collimation interferometry. This chapter will discuss the technical principles and features of two representative product families: the HEIDENHAIN LIP series and the Sony Magnescale series.

3.2. Dual-Grating Interferometry and Optical Frequency Multiplication

Figure 4a,b illustrate diffraction-order coupling in a representative dual-grating system and a representative single grating interferometric configuration, respectively [1]. Heidenhain's LIP series stands as a prominent example of interferential scanning technology, with its core operating on the dual-grating interference principle [45]. By virtue of an innovative optical configuration, the series realizes optical frequency multiplication, enabling nanometer to sub-nanometer measurement steps and exceptional system accuracy within a compact form factor.

The LIP series interferential scanning linear encoders employ LEDs as the light source, and their operating principle is based on dual-grating interference. The beam experiences two successive diffractions between the scanning grating and the scale grating. By exploiting the variation in phase difference when the ±1st-order diffracted beams interfere, optical frequency doubling is realized, yielding a signal period of half the grating pitch. Through the Heidenhain Signal Processing (HSP) 1.0 Application-specific integrated circuit (ASIC), the scanning signals are continuously monitored. When signal amplitude decreases, the

ASIC compensates by increasing the LED current, thereby ensuring ideal signal waveforms and stable signal quality even under contamination.

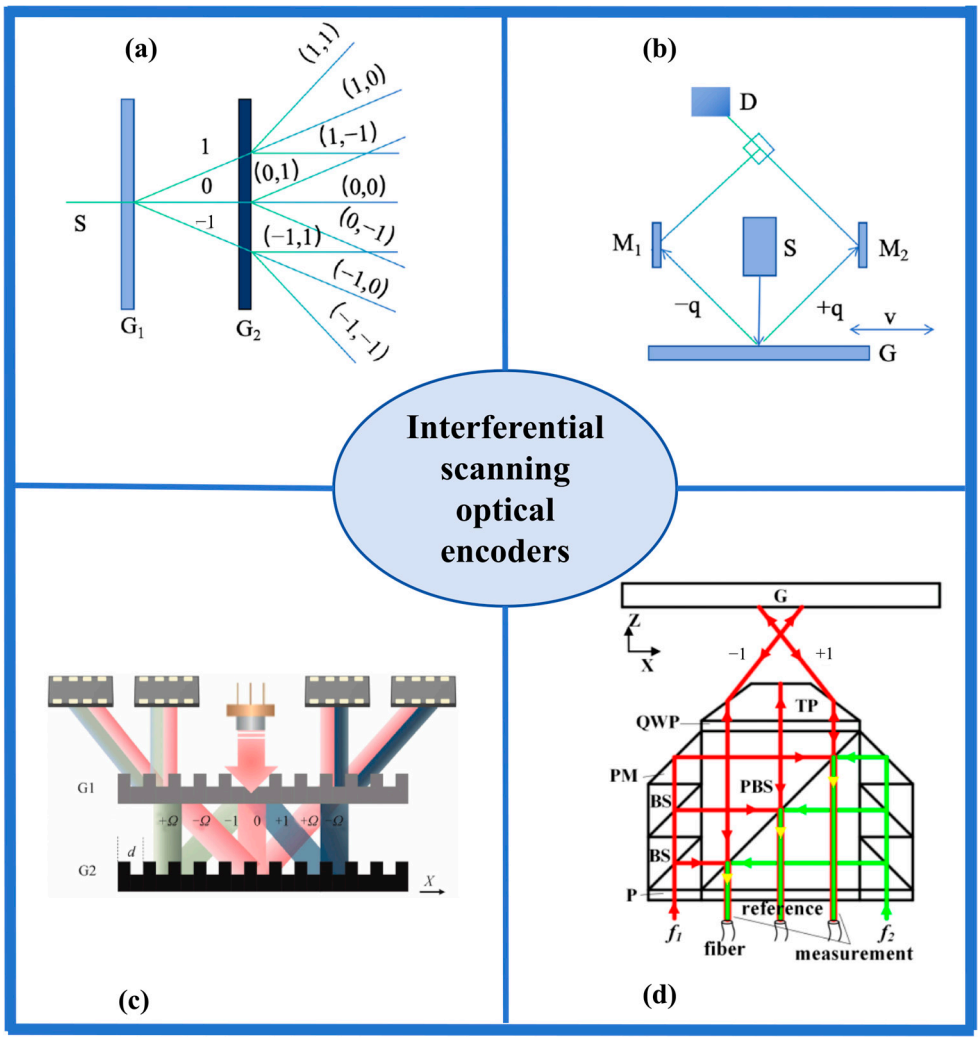


Figure 4. Representative operating principles and optical configurations of interferometric scanning grating encoders: (**a**) diffraction-order coupling in a dual-grating system; (**b**) single-grating interferometric configuration; (**c**) triple-diffraction optical path in a dual-grating encoder; and (**d**) optical configuration of a two-degree-of-freedom fiber-coupled heterodyne grating interferometer. Panels (**a**–**c**) were adapted from Ref. [1], and panel (**d**) was adapted from Ref. [63].

To further enhance resolution, Heidenhain incorporated a more sophisticated optical architecture in its premium model LIP 382 [64], achieving optical quadrupling and beyond. Figure 4c presents a representative triple-diffraction optical path in a dual-grating encoder [1]. The LIP 382 optical architecture employs an interferential scanning architecture that relies on cascaded diffraction between an index grating and a scale grating. The collimated beam from the source impinges on the index grating, producing multiple diffraction orders. The ±1st order diffracted beams subsequently reach the scale grating and undergo a second diffraction, and the two beams overlap spatially to generate interference fringes. For each grating pitch of relative displacement of the scale grating, the interference signal completes four full periods, meaning the effective signal period is reduced to a quarter of the scale grating pitch, thus realizing optical division. The interference intensity is converted by a photodetector array into quadrature electrical output signals. The common-path configuration effectively eliminates environmental disturbances as common-mode noise, thereby realizing a stable optical basis for high-resolution displacement metrology.

3.3. Holographic Grating and Grating Interferometry

The Sony Magnescale laser scale employs a holographic-grating-based interferometric configuration. A volume holographic grating together with a polarization beam splitter (PBS) is used for beam separation and polarization conversion, while optical quadruple frequency multiplication is achieved via double diffraction [65].

In the Sony configuration, the beam from a semiconductor laser is divided by a polarization beam splitter into S-polarized and P-polarized components, both of which are subsequently diffracted by a volume holographic grating featuring exceptionally high diffraction efficiency. The two diffracted beams travel through respective quarter-wave plates ($\lambda/4$ plates) to mirrors, which reflect the beams back through the quarter-wave plates a second time. This process transforms S-polarized light into P-polarized light, and conversely converts P-polarized light into S-polarized light. The two beams undergo diffraction once more by the volume holographic grating, after which they are recombined by the polarization beam splitter to generate interference. Due to the polarization switching, all interfering light is directed toward the photodetector. Since double diffraction adds phases of +2Kx and -2Kx to the respective beams, every increment of one grating pitch results in four alternating bright–dark cycles in the interference signal. Thus, for a grating pitch of 0.55 μm, the effective signal pitch becomes 0.55/4 = 0.138 μm.

Owing to the high spatial symmetry between the measurement and reference optical paths, which share a common laser source and the same volume holographic grating, any fluctuations in laser wavelength or air refractive index induced by temperature or pressure variations result in identical phase perturbations on both optical paths. Upon differential interferometric detection following recombination at the polarization beam splitter, this common-mode disturbance is inherently nulled, allowing the system to sustain sub-nanometer stability under routine operating conditions without requiring external environmental compensation. This constitutes the fundamental optical principle behind its self-calibration capability.

Figure 4d shows a representative two-DOF fiber-coupled heterodyne grating interferometer [63]. Two optical frequencies, f_1 and f_2, are introduced into the encoder head, where polarization beam splitters, quarter-wave plates, and a reflective grating are used to form measurement and reference interference signals. The measured phase variations are then used to obtain the in-plane and out-of-plane displacements.

3.4. Interferential Scanning Absolute Grating Encoders

Sony once introduced a two-dimensional (2D) absolute-position measurement concept in the XY plane utilizing a variable-pitch grating [66]. The approach achieves absolute position determination using a variable-pitch grating and two reading heads. The grating pitch of the 2D grating exhibits a quadratic polynomial spatial distribution, while the two reading heads are kept a constant distance apart. As each reading head performs scanning with a step corresponding to the central grating pitch, the interference signal period directly correlates with the local grating pitch. Consequently, the two reading heads yield distinct output values that vary according to a quadratic polynomial function. Subtracting the two reading head outputs yields a linear term. This difference, when compared with pre-calibrated position data, allows absolute displacement measurement. The system attains measurement accuracy better than $\pm$50 nm within a 280 mm $\times$ 300 mm range.

Hence, by harnessing the diffraction and interference effects of gratings, interferential scanning encoders realize optical subdivision directly at the signal origin, thereby resolving the inherent conflict between resolution and speed that characterizes conventional imaging scanning techniques. The dual-grating interference and optical frequency multiplication of Heidenhain's LIP series, together with the holographic grating and self-aligned optical

configuration of Sony Magnescale, exemplify distinct technological pathways toward high precision and high stability, respectively. At present, interferential scanning technology has established itself as the dominant approach for sub-nanometer displacement metrology. Table 2 presents a comparative summary of the key performance specifications of the representative interferential scanning encoders from each manufacturer discussed above. It clearly demonstrates the marked superiority of interferential scanning technology in attaining picometer-scale resolution.

Table 2. Key performance parameters of representative interferential scanning grating encoders from major manufacturers.

Product Models	Manufacturers	Type	Max. Range	Max. Resolution	Max. Speed
LIP	Heidenhain	Incremental	3040 mm	<0.1 nm	10 m/s
BS78	Magnescale	Incremental	420 mm	2.1 pm	400 mm/s
BH25	Magnescale	Incremental	420 mm	3.8 pm	1800 mm/s
BL57	Magnescale	Incremental	1060 mm	10 nm	3000 mm/s
BL50H	Magnescale	Incremental	500 mm × 600 mm	6.1 pm	5 m/s

4. Multi-DOF Grating Interferometer Systems

With the growing demand for motion degrees of freedom in precision manufacturing, semiconductor equipment, and optical platforms [67–70], encoder technology has steadily advanced from early linear encoders [71] toward multi-DOF systems [72]. This evolution has yielded a comprehensive technological landscape encompassing two-dimensional planar measurement [73–76], three-dimensional spatial positioning [77–80], and six-DOF measurement [81–83]. Using Sony and Heidenhain products as illustrative examples, this chapter systematically presents the principles and technical realizations of interferometric measurement for Z-axis displacement, in-plane XY motion, out-of-plane XZ/YZ displacement, integrated three-DOF sensing, and six-DOF pose determination.

4.1. Subsystem-Level Interferometric Measurement Schemes

It is worth noting that Sony has carried out substantial foundational research and prototype validation in the field of multi-DOF grating interferometry. Several of the systems discussed in this section, including the XZ two-DOF system and the three-DOF integrated system, are drawn mainly from Sony's publicly accessible technical materials, patent publications, and academic literature [84–86]. Even so, these approaches offer significant insights in optical configuration and decoupling algorithms, representing important technological directions in this domain.

Figure 5 summarizes representative multi-DOF grating-interferometric configurations, including two-axis surface encoding, XY in-plane measurement, XZ in-/out-of-plane measurement, and integrated XYZ displacement measurement.

4.1.1. Z-Axis Single-Degree-of-Freedom Displacement Measurement Systems

In applications including multilayer structure inspection and surface profilometry, Z-axis displacement (perpendicular to the measurement plane) is of critical importance. Sony's Z-axis interferometric system adopts a common-path differential interference architecture, which provides both high resolution and robust rejection of environmental perturbations.

Sony proposed a Z-axis common-path differential grating interferometer [84]. The system utilizes a multimode semiconductor laser having a center wavelength of 781 nm. The emitted laser beam is divided by a PBS into a reference path and an object path.

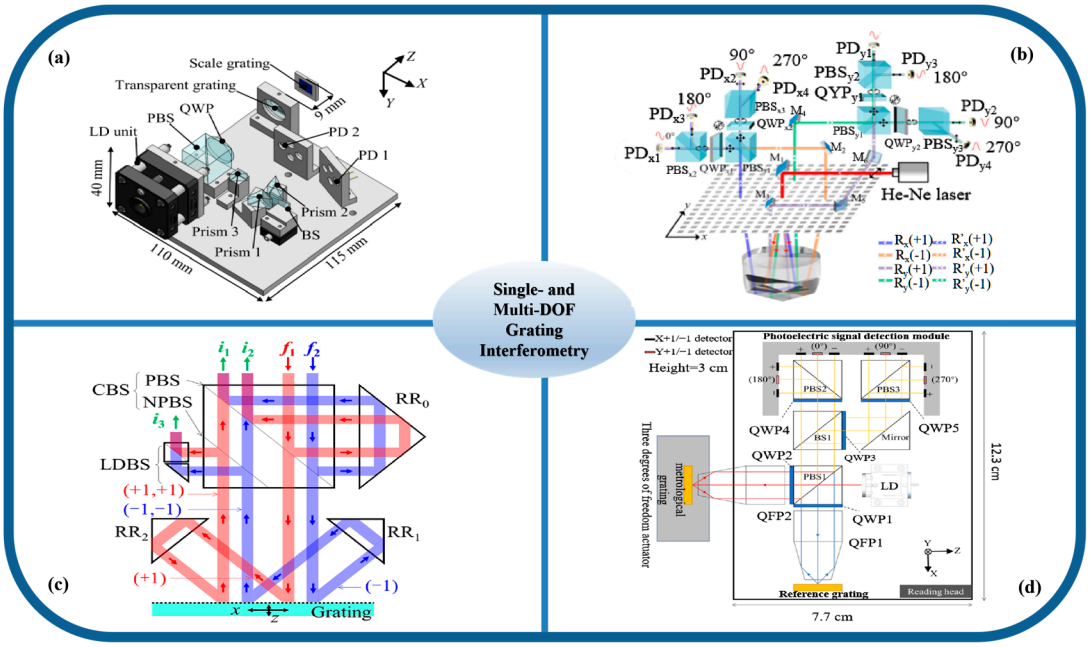


Figure 5. Representative multi-DOF grating-interferometric configurations: (**a**) overall structural configuration of a prototype two-axis surface encoder for simultaneous in-plane X-directional and out-of-plane Z-directional displacement measurements [69]; (**b**) two-dimensional grating interferometer for simultaneous X- and Y-direction displacement measurements [74]; (**c**) spatially separated heterodyne grating interferometer for simultaneous in-plane X- and out-of-plane Z-direction displacement measurements [75]; and (**d**) compact XYZ three-DOF grating encoder based on quadrangular frustum pyramid prisms [77]. Panels (**a**–**d**) were adapted from Refs. [69,74,75,77], respectively.

In the reference arm, P-polarized light travels sequentially via a mirror reflection, diffraction by a holographic grating, transmission through a quarter-wave plate, and finally retroreflection by a right-angle mirror. As the beam traverses the quarter-wave plate twice, its polarization flips from P to S, preventing feedback into the laser. The holographic grating remains stationary and does not contribute to phase modulation. In the object arm, S-polarized light impinges on the movable mirror (the measurement target). Following reflection from the mirror and diffraction by the same holographic grating, it is likewise retroreflected by the right-angle mirror. The two beams recombine at the PBS and interfere. The resulting interference signal is demodulated by a detection module comprising a quarter-wave plate, a non-polarizing beam splitter (BS), a PBS, and four photodetectors, ultimately yielding Z-axis displacement data.

The essence of this approach resides in its common-path differential interferometric configuration. Since the measurement and reference beams share the same holographic grating and the majority of optical elements, environmental disturbances are effectively canceled as common-mode noise by the differential architecture. This allows high-precision, stable measurements to be performed in ordinary laboratory settings without requiring rigorous environmental isolation.

For comparison, Figure 5a presents the overall structural configuration of a prototype two-axis surface encoder integrating the optical components required for simultaneous in-plane X-directional and out-of-plane Z-directional displacement measurements [69].

4.1.2. XY In-Plane Two-Dimensional Displacement Measurement Systems

Planar motion stages demand high-precision X/Y displacement detection. Sony introduced an XY two-DOF system that utilizes a two-dimensional planar grating together with dual interferometric optical paths for decoupled measurement. In the Sony system, the X-

axis detection channel operates as follows, while the Y-axis configuration is analogous [85]: the 2D grating scale is oriented perpendicular to the XZ plane to measure displacement along the X-axis. The system employs a 790 nm multimode semiconductor laser. The output beam is divided by a PBS into S- and P-polarized components, which are directed onto the grating at a prescribed angle. The two diffracted beams traverse quarter-wave plates, are retroreflected by mirrors with their polarizations exchanged, experience a second diffraction, recombine at the PBS, and finally reach the photodetector. The optical configuration spatially separates the forward and return beam paths, thereby mitigating feedback interference. By equalizing the optical path difference between the two arms to within a few micrometers—monitored in real time using a low-coherence laser—the influences of source wavelength drift and refractive index variations induced by temperature, pressure, and humidity changes are largely nullified, yielding outstanding long-term stability. Through double diffraction, optical quadrature frequency multiplication is realized, reducing the signal period to a quarter of the grating pitch. This provides the physical basis for sub-nanometer resolution. Figure 5b shows another similar representative two-dimensional grating interferometer, in which a transmissive two-dimensional grating and a corner-cube retroreflector are used to form orthogonal X- and Y-direction measurement channels [74].

4.1.3. XZ In-/Out-of-Plane Two-Degree-of-Freedom Displacement Measurement Systems

In applications where both in-plane and out-of-plane displacements need to be measured simultaneously, XZ or YZ two-DOF systems enable concurrent detection of one horizontal axis and the vertical axis.

Sony also developed an XZ two-degree-of-freedom grating interferometer for simultaneous in-plane X-axis and out-of-plane Z-axis displacement measurement [86]. Following beam splitting by the PBS, the measurement beam undergoes diffraction at the grating, generating $\pm$1st-order diffracted beams. These beams are then retroreflected by a transmissive volume holographic grating, thereby achieving two successive interactions with the grating. The reference beam traverses a comparable path using a separate reference grating together with the same volume holographic grating. Upon return, the two beams recombine and interfere, with the resulting phase being jointly modulated by both X-axis and Z-axis displacements.

The interference light is split by polarization optics into four signals in phase quadrature. Through subsequent signal processing, the X and Z displacement components are decoupled and extracted. This system likewise employs a laterally displaced optical configuration to prevent feedback interference, while the incorporation of a holographic grating enhances both diffraction efficiency and optical stability. Figure 5c shows another simialr representative XZ two-DOF implementation based on spatially separated heterodyne grating interferometry [75].

4.1.4. XYZ Three-Degree-of-Freedom Integrated Measurement Systems

To realize full-parameter precision measurement in three-dimensional XYZ space, the aforementioned subsystems may be integrated. Sony has presented two representative three-DOF integrated architectures in its publicly disclosed technical materials: (1) XY system + Z system, where the XY in-plane system (Section 4.1.2) and the Z-axis system (Section 4.1.1) are combined, employing separate reading heads to measure in-plane and out-of-plane displacements independently; (2) XZ system + YZ system: two out-of-plane systems are placed orthogonally, and three-dimensional displacement is determined via data fusion [86].

By augmenting the XZ-axis grating interferometer with a second grating interferometer—rotated by 90° around the Z-axis for YZ-axis displacement detection—Y-

axis displacement can likewise be measured in a two-dimensional configuration. Moreover, it is possible to align the sensing location of the XZ-axis interferometer with that of the YZ-axis interferometer. Under this condition, employing such an orthogonal arrangement enables a three-dimensional encoder that measures displacements along the X, Y, and Z axes. Figure 5d shows another similar compact XYZ three-DOF implementation based on quadrangular frustum pyramid prisms, integrating the X-, Y-, and Z-direction measurement channels within a single reading head [77].

According to Sony's publicly disclosed technical materials, both the approach that combines an XY-axis grating interferometer with a Z-axis grating interferometer, and the approach that employs XZ-axis interferometers for YZ-axis displacement detection, are viable for realizing three-dimensional encoders. Of these, the XY system + Z system offers better performance in high accuracy, high resolution, and long-term stability. This modular architecture not only lowers the complexity of system development but also permits flexible combination of different subsystems tailored to specific application needs, thereby trading off performance and cost effectively.

4.2. In-Plane Two-Dimensional Measurement Schemes

Beyond Sony, Heidenhain's KGM series [87] offers a high-performance in-plane two-DOF measurement solution. The principle of this series is largely identical to that of the two-DOF grating interferometer [88].

Both systems are founded on single-frequency laser homodyne interferometry. A two-dimensional diffraction grating having consistent groove geometry in two orthogonal directions is employed. Phase changes arising from Doppler frequency shifts are acquired in each diffraction direction, enabling the determination of X and Y displacements. A representative two-dimensional grating-interferometric readout configuration is shown in Figure 6b [74].

Additionally, Heidenhain has developed a two-coordinate incremental grating scale, the PP281 [45], designed for in-plane two-DOF measurement. A simplified schematic based on the operating principle of this type of planar XY grating encoder is shown in Figure 6a. This device offers a measurement accuracy of ± 2 μm, a 68 mm $\times$ 68 mm measurement range, and a measurement step adjustable from 1 μm down to 0.05 μm. The representative planar two-degree-of-freedom systems discussed above, together with the three-DOF and higher-DOF grating measurement systems introduced in Sections 4.3 and 4.4, are summarized in Figure 6.

4.3. Three-DOF Measurement with a Zero-Dead-Zone Heterodyne Grating Interferometer

Beyond the aforementioned commercialized schemes, important advances have likewise been made in academic research on grating interferometry. Responding to the demanding requirements of next-generation lithography systems and atomic-scale manufacturing for multi-DOF displacement metrology, Li Xinghui and co-workers have proposed a new integrated heterodyne grating interferometer [68]. The optical architecture of this system is illustrated in Figure 6e. After passing through a polarization beam splitter, the dual-frequency laser beam is directed to the measurement grating and the reference grating, respectively. The ± 1st-order diffracted beams undergo multiple reflections and polarization transformations, after which they are combined to produce interference, yielding five heterodyne signals. These signals are then processed in real time by a field-programmable gate array (FPGA), enabling the extraction of three-DOF displacement data.

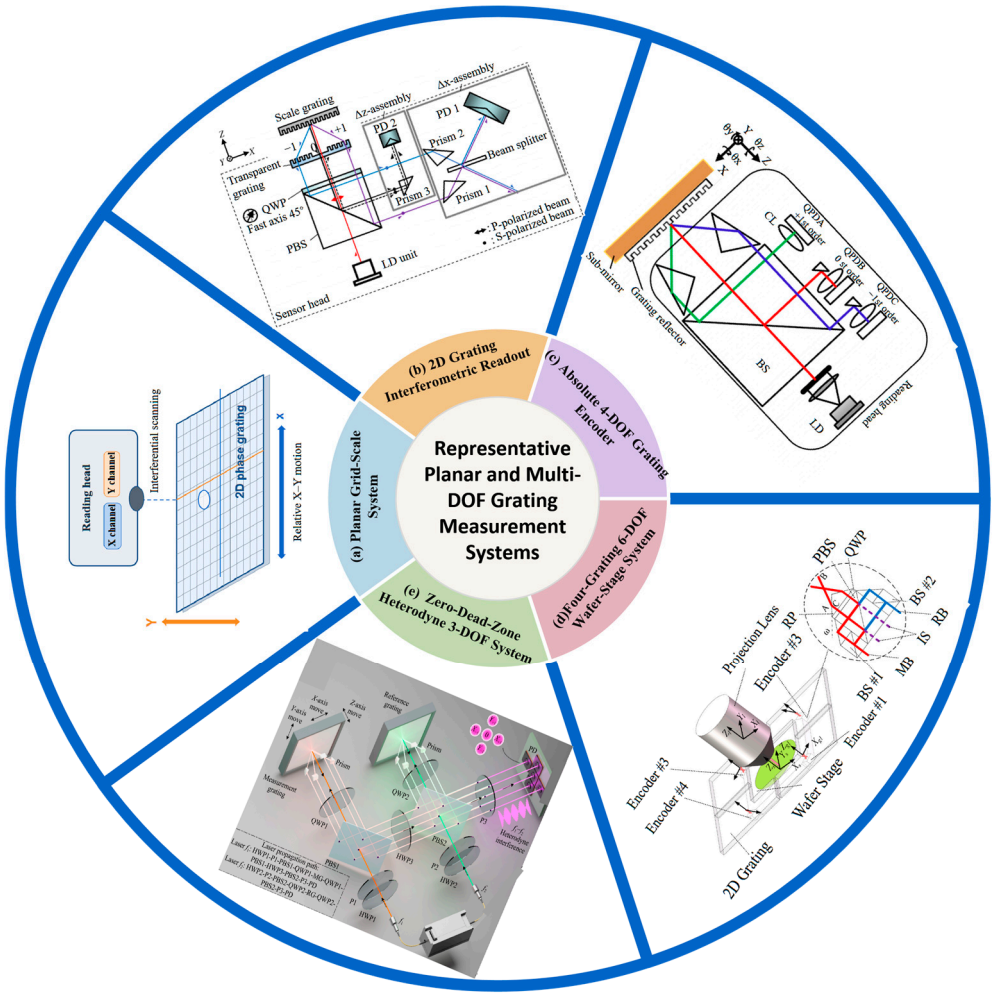


Figure 6. Representative planar and multi-DOF grating measurement systems: (**a**) simplified schematic of a planar XY grating encoder, redrawn by the authors based on the operating principle of the HEIDENHAIN PP281 [45]; (**b**) two-dimensional grating-interferometric readout configuration [74]; (**c**) absolute four-DOF grating encoder [70]; (**d**) four-grating interferometer system for six-DOF wafer-stage displacement measurement [89]; and (**e**) zero-dead-zone heterodyne three-DOF grating interferometer [68].

This system utilizes a dual-frequency laser source together with a compact, zero-dead-zone optical configuration. A spatially symmetric optical path design cancels the optical path difference between the reference and measurement arms, consequently suppressing phase errors caused by air refractive index variations and laser frequency drift. The laboratory prototype has dimensions of 90 mm × 90 mm × 40 mm and enables simultaneous displacement measurement along the X, Y, and Z axes. The system offers a resolution of 0.25 nm along X and Y and 0.3 nm along Z. The linearity errors are better than 6.9×10^{-5} (X), 8.1×10^{-5} (Y), and 16.2×10^{-5} (Z). Over a 1000 s duration, the stability is better than 20 nm in the XY plane and 60 nm along the Z-axis. Moreover, the system incorporates crosstalk error analysis together with compensation algorithms, effectively suppressing multi-axis coupling errors to below 5%.

This work demonstrates the viability of heterodyne interferometry combined with a compact optical architecture for multi-DOF measurement, offering an alternative high-precision, compact approach for multi-DOF grating interferometry that usefully complements the commercialized schemes discussed earlier.

4.4. Multi-DOF Surface Encoder

The sensing head of the six-degree-of-freedom surface encoder developed by Gao Wei and co-workers [90] comprises a displacement-module assembly [91] and an angle-module assembly [92]. The displacement module operates on the principle of a three-axis displacement sensor and measures translational motions X, Y, and Z. The angle module, founded on the principle of a three-axis autocollimator, measures angular motions (pitch, yaw, and roll). The displacement module and the angle module of the six-degree-of-freedom surface encoder share the same laser source and are integrated into a single sensor assembly through a compact optical layout, enabling six-degree-of-freedom measurement.

The laser source comprises a laser diode paired with a collimating lens, producing a collimated output beam. The collimated beam first traverses beam splitter 1 (BS1) and is then divided by beam splitter 2 (BS2) into two paths: one illuminates the scale grating, the other illuminates the reference grating. The scale grating and the reference grating share an identical grating period g along both the X and Y axes. Each grating independently produces +1st-order diffracted beams along the X and Y directions at a diffraction angle θ. The diffracted beam from the scale grating is reflected by BS2, whereas that from the reference grating transmits through BS2. These two diffracted beams interfere with each other. The resulting interference signals are detected by four independent photodiodes (PD units A, B, C, D) and subsequently used to extract displacement information along the X, Y, and Z axes.

For angular displcement measurement, the 0th-order diffracted light and the −1st-order diffracted light (in the X direction) from the scale grating pass through BS2 into the angle measurement module. Within this module, the beam reflected by BS1 is directed to two autocollimator units. Each autocollimator unit comprises a collimating lens and a four-quadrant photodiode (QPD), labeled QPD C and QPD D, respectively. These units serve to detect the angular motion of the target object. The complete optical system is integrated within a single assembly, enabling simultaneous multi-DOF measurement of both translation and angular motion.

Figure 6c presents another representative absolute four-DOF grating encoder capable of measuring Z-axis displacement together with rotations about the X, Y, and Z axes [70]. At the system level, Figure 6d shows a four-grating interferometer arrangement in which four two-DOF encoders are distributed around a wafer stage to reconstruct its six-DOF displacement relative to the projection lens [89].

5. Self-Calibration of Diffraction Gratings

For high-precision optical encoders, the grating serves not only as the element that generates the reading signal, but also as the spatial reference for displacement measurement. Pitch deviation and out-of-flatness of the grating can influence the reading signal, thereby affecting the linearity, repeatability, and positioning accuracy of the encoder [32]. Therefore, grating calibration after manufacturing is an important step in the quality control of high-precision encoders. Recently, self-traceable nanograting fabrication based on scanning and splicing atom lithography has been demonstrated, enabling the production of large-area, high-uniformity sub-micron pitch gratings, which provides a new process pathway for improving the original quality of encoder gratings [27].

Existing grating calibration methods can be broadly divided into whole-scale calibration, local calibration, and full-field interferometric calibration. Linear comparators and vacuum interferometric comparators provide high accuracy for one-dimensional linear scales, but their system structures are complex and their calibration efficiency is limited [93]. Microscopy and atomic force microscopy (AFM) can observe local line morphology or local pitch variation, but they are not suitable for full-field calibration. In contrast, Fizeau-

interferometer-based methods use diffracted wavefronts from different diffraction orders and are therefore suitable for planar scale gratings, long-range linear scales, and variable-line-spacing (VLS) gratings.

5.1. Self-Calibration of Planar Scale Gratings with Constant Pitch Using Fizeau Interferometry

For planar scale gratings, both pitch deviation and out-of-flatness can affect the diffracted wavefront and thus the encoder performance. Gao and Kimura first proposed a fast evaluation method for pitch deviation and out-of-flatness [94]. Chen et al. subsequently proposed a Fizeau-interferometer-based self-calibration method for planar scale gratings [95], and Xiong et al. further evaluated the associated measurement uncertainty [96]. As shown in Figure 7, the zeroth-order diffracted wavefront is used for out-of-flatness evaluation, whereas the first-order diffracted wavefront is used for pitch-deviation evaluation. This approach enables full-field calibration of planar scale gratings by linking the diffracted wavefront information to the geometric errors of the grating.

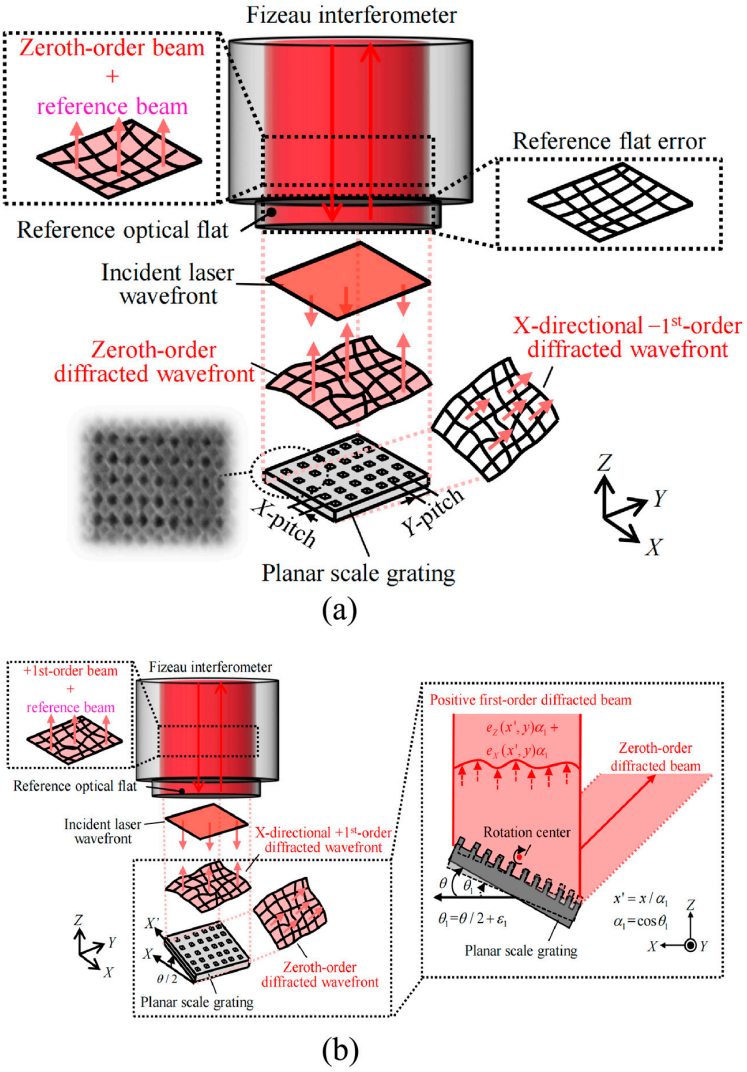


Figure 7. Fizeau-based calibration principles for a planar scale grating: (**a**) zeroth-order diffracted wavefront measurement for out-of-flatness evaluation; (**b**) positive first-order diffracted wavefront measurement for pitch-deviation evaluation [96].

Figure 8 shows representative calibration results of a planar scale grating. The Z-directional out-of-flatness is presented in Figure 8a, whereas the X- and Y-directional pitch deviations are shown in Figure 8b,c, respectively. These results demonstrate that the Fizeau-

based method can provide full-field error maps for planar scale grating calibration and can separately characterize out-of-flatness and pitch deviations along different directions [96].

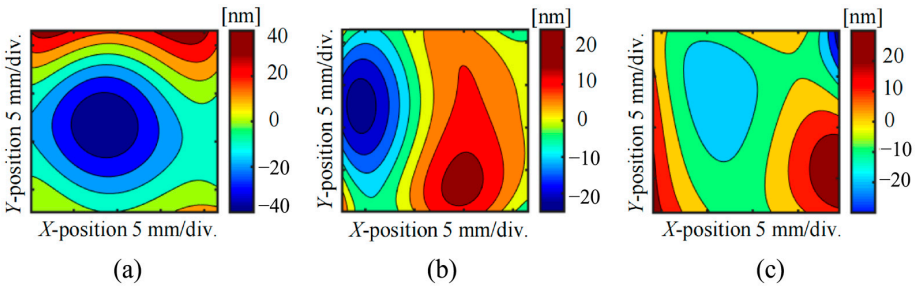


Figure 8. Representative calibration results of a planar scale grating using Fizeau interferometry: (**a**) Z-directional out-of-flatness; (**b**) X-directional pitch deviation; (**c**) Y-directional pitch deviation [96].

5.2. Self-Calibration of Interferometer and Planar Scale Gratings

In high-precision calibration, the error of the Fizeau reference flat could be comparable to the grating error and therefore cannot be ignored. Chen et al. proposed a self-calibration method for a Fizeau interferometer and planar scale gratings in the Littrow setup [95]. By incorporating the reference-flat error into the calibration model, this method separates the grating error from the Fizeau reference-flat error within the same measurement framework. Xiong et al. further evaluated the uncertainty of this calibration method [96] and extended the idea to pitch deviation calibration of linear scales [97].

5.3. Stitching Self-Calibration of Long-Range Linear Scales

A single Fizeau field of view is limited, whereas engineering linear scales often require long calibration ranges. Xiong et al. proposed a self-calibration stitching method for pitch deviation evaluation of a long-range linear scale [98]. As shown in Figure 9, the one-shot measurement result and the three-shot stitching result show good agreement, indicating that stitching can extend the calibration range while maintaining reliable pitch deviation evaluation. Since stitched results may be affected by subaperture registration, low-order error correction, and global error propagation, these factors still need to be considered [99].

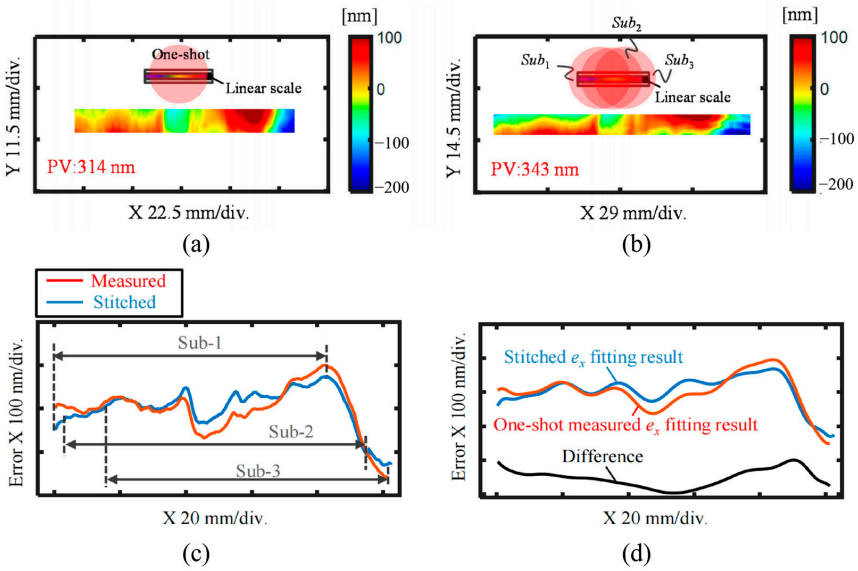


Figure 9. Comparison of one-shot measurement and stitching calibration results for a long-range linear scale: (**a**) pitch deviation map obtained by one-shot measurement; (**b**) pitch deviation map obtained by three-shot stitching measurement; (**c**) comparison between measured and stitched error profiles; (**d**) fitted error profiles and their difference [98].

5.4. Self-Calibration of Large-Scale Two-Dimensional Gratings in Absolute Encoders

For absolute encoders, VLS gratings provide a position-dependent coding reference rather than a constant-pitch reference. Related studies have introduced absolute optical imaging encoders and variable-period planar scale gratings for absolute position encoding [100,101]. For the calibration of VLS gratings, Xiong et al. proposed a Fizeau-interferometer-based self-calibration method [102].

For large-scale two-dimensional VLS gratings, the limited field of view of a single Fizeau interferometer becomes increasingly significant. We proposed a self-calibration method for large-scale VLS gratings by differencing spatially shifted phase maps [103]. As shown in Figure 10, the X- and Y-directional pitch distributions and their corresponding central cross-sectional profiles were reconstructed over a large two-dimensional measurement area. Figure 10a,b show the evaluated pitch distribution and central cross-sectional profile in the X-direction, whereas Figure 10c,d present the corresponding results in the Y-direction. These results demonstrate the feasibility of the proposed method for calibrating large-scale two-dimensional VLS gratings. Yin et al. further proposed a conjugate differential self-calibration method for large-scale two-dimensional VLS gratings [104]. The reconstructed pitch variations showed good agreement with the encoder calibration results, indicating that these methods can provide reliable calibration data for error compensation in absolute optical encoders.

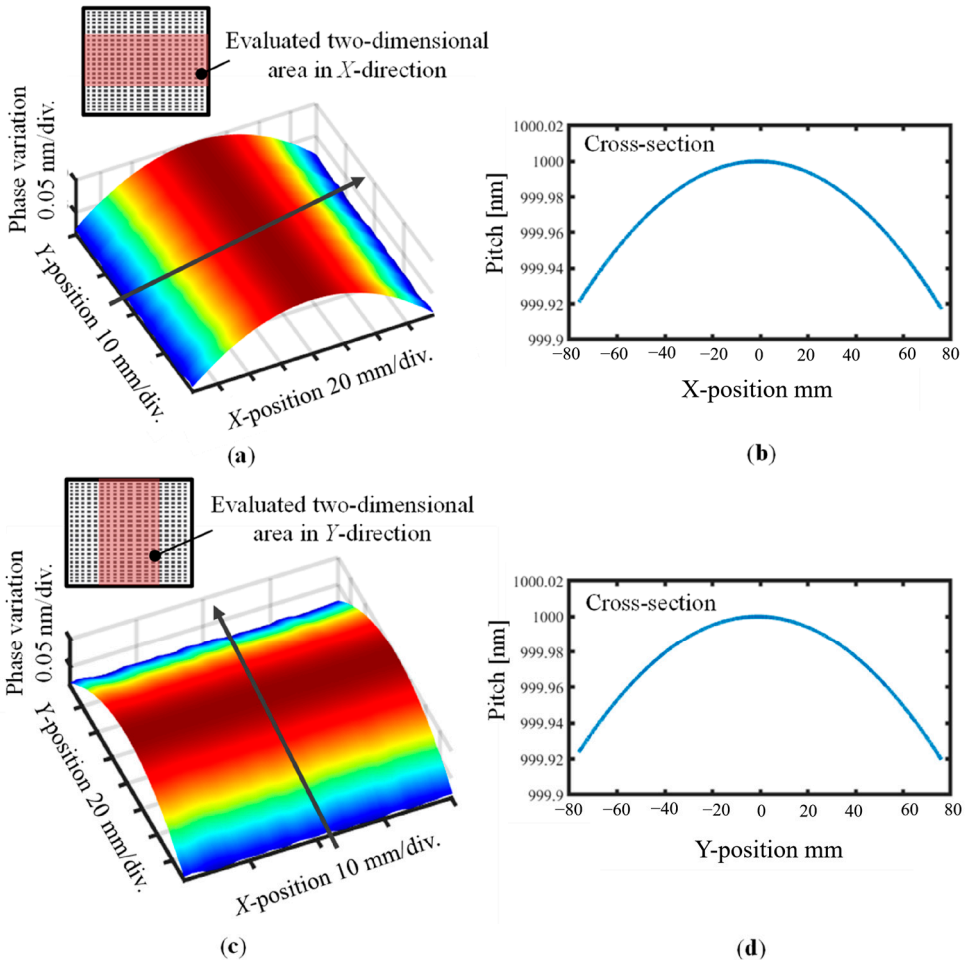


Figure 10. Evaluated pitch distributions of a large-scale two-dimensional VLS grating: (**a**) X-directional evaluated area and pitch distribution; (**b**) X-directional central cross-sectional pitch profile; (**c**) Y-directional evaluated area and pitch distribution; (**d**) Y-directional central cross-sectional pitch profile [103].

6. Conclusions

This review has systematically charted the technological evolution of grating encoders, from imaging scanning to interferential scanning, from incremental to absolute encoding, and from single-DOF to multi-DOF integration, focusing on commercial products and complementing them with academic advances and grating characterization techniques.

Imaging scanning encoders effectively improve signal fidelity and immunity to disturbances by means of single-field scanning, spatial filtering, and multi-fringe averaging. Absolute encoders, through multi-track encoding or single-track pseudo-random coding strategies, concurrently deliver nanometer-scale resolution and measurement speeds on the order of meters per second without needing a reference return procedure. Interferential scanning encoders, by contrast, realize optical subdivision via diffractive interference, reducing the effective signal period to one-half, one-quarter, or an even smaller value of the physical grating pitch. This provides the physical basis for picometer-scale metrology. In the multi-DOF domain, commercial solutions already address in-plane two-dimensional measurement, whereas academic endeavors, including zero-dead-zone heterodyne three-DOF grating interferometers and six-DOF surface encoders, have pushed the technological frontiers further. Moreover, grating characterization techniques employing a Fizeau interferometer have been extended from planar grating evaluation to the calibration of long-stroke linear gratings and variable-pitch gratings, thereby supporting error compensation in absolute encoders.

Despite the considerable progress achieved in grating encoder technology, several challenges remain. The principal bottlenecks are the fabrication yield and cost of large-format, highly uniform sub-micrometer pitch gratings, together with the dynamic modeling and real-time compensation of crosstalk errors in multi-DOF measurement. Additionally, preserving accuracy uniformity across extremely long measurement ranges remains an urgent problem to be addressed.

From an industrial application perspective, the performance priorities and engineering constraints of grating encoders vary considerably across different scenarios. In semiconductor manufacturing equipment, wafer stages and alignment systems often require nanometer-level positioning, high-speed response, compact multi-DOF integration, and effective compensation for thermal drift and inter-axis crosstalk. In ultra-precision machine tools, major challenges include maintaining measurement accuracy and robustness over long travel ranges under vibration, contamination, temperature variation, and mounting errors, while controlling system cost and facilitating in situ calibration. For precision instruments, grating encoders generally need to provide long-term dimensional stability, traceable calibration, and reliable linear and angular displacement measurements over large strokes, where environmental disturbances, structural deformation, and multi-axis error accumulation can become particularly significant. Consequently, the industrial deployment of next-generation grating encoders is likely to depend not only on improvements in nominal resolution but also on system-level integration, environmental robustness, practical self-calibration strategies, and long-term reliability.

Looking ahead, grating encoder technology is expected to advance toward enhanced performance, higher integration, and increased intelligence. The primary developmental pathways for grating encoder technology will include the adoption of novel materials to simplify optical architecture, the introduction of new operating principles to increase information capacity, and the integration of intelligent algorithms for self-calibration and predictive maintenance.

https://doi.org/10.3390/photonics13080735

Author Contributions: Conceptualization, X.X.; methodology, X.X.; software, X.X.; validation, X.X., Y.Y. and Y.Z.; formal analysis, X.X., Y.Z. and B.X.; investigation, X.X., Y.Z. and Y.Y.; resources, X.X.; data curation, X.X., Y.Z., K.W. and Y.Y.; writing—original draft preparation, X.X., Y.Z. and B.X.; writing—review and editing, Y.Z., B.X., K.W. and X.X.; visualization, X.X.; supervision, X.X.; project administration, X.X.; funding acquisition, X.X. All authors have read and agreed to the published version of the manuscript.

Funding: This research was funded by National Natural Science Foundation of China, Grant No. 52505588, 52475549, the National Key R&D Program of China, Grant No. 2024YFB3312701, the Science and Technology Research Program of Chongqing Municipal Education Commission, Grant No. KJQN202401123.

Informed Consent Statement: Not applicable.

Data Availability Statement: The datasets generated and analyzed for this study are available from the corresponding author on reasonable request.

Conflicts of Interest: The authors declare no competing interests.

References

1. Cui, C.; Li, X.H. Precision Nanometrology: Laser Interferometer, Grating Interferometer and Time Grating Sensor. *Sensors* **2025**, *25*, 6791. [CrossRef] [PubMed]
2. Shi, Y.; Xu, Z.; Wu, J.; Chen, L.; Liang, Y.; Sun, Q.; Zhou, Z. Ultra-Low Frequency High-Precision Displacement Measurement Based on Dual-Polarization Differential Fiber Heterodyne Interferometer. *J. Light. Technol.* **2023**, *41*, 5773–5779. [CrossRef]
3. Liu, H.; Lu, B.; Jiang, Z. Grating Interference Ultra-Precision Measurement Technology Applied to High-End Equipment. *Engineering* **2025**, *61*, 333–353. [CrossRef]
4. Yang, M.; Cui, C.; Liu, L.; Zhao, P.; Gao, L.; Li, X. An unfolding-based model for analysis of rotation and translation coupling in grating interferometers. In *Proceedings of the Advanced Sensor Systems and Applications XIV*; SPIE: California, CA, USA, 2024; pp. 56–65.
5. Kimura, A.; Gao, W.; Arai, Y.; Lijiang, Z. Design and construction of a two-degree-of-freedom linear encoder for nanometric measurement of stage position and straightness. *Precis. Eng.* **2009**, *34*, 145–155. [CrossRef]
6. Kang, J.; Zhong, L.; Hao, B.; Su, Y.; Zhao, Y.; Yan, X.; Hao, S. A novel linear displacement sensor based on double-threshold decoding algorithm. *Sens. Rev.* **2024**, *44*, 1–12. [CrossRef]
7. Lim, H.; Shimizu, Y. Feasible Resolution of Angular Displacement Measurement by an Optical Angle Sensor Based on Laser Autocollimation. *Nanomanuf. Metrol.* **2023**, *6*, 32. [CrossRef]
8. Zhan, B.; Wu, C.; Liu, X.; Huang, P.; Yu, P. An integrated high precision absolute angular displacement sensor. *Meas. Sci. Technol.* **2024**, *35*, 095105. [CrossRef]
9. George, B.; Tan, Z.; Nihtianov, S. Advances in Capacitive, Eddy Current, and Magnetic Displacement Sensors and Corresponding Interfaces. *IEEE Trans. Ind. Electron.* **2017**, *64*, 9595–9607. [CrossRef]
10. Wang, S.C.; Xie, B.R.; Huang, S.M. Design and Analysis of Small Size Eddy Current Displacement Sensor. *Sensors* **2022**, *22*, 7444. [CrossRef] [PubMed]
11. Xue, X.; Dong, Y.; Wu, X. Motion Induced Eddy Current Sensor for Non-intrusive Vibration Measurement. *IEEE Sens. J.* **2020**, *20*, 735–744. [CrossRef]
12. Xu, C.M.; Yuan, S.; Liu, M.J. Design and analysis of an eddy current displacement sensor with extended linear range. *Sens. Actuator A-Phys.* **2024**, *368*, 11. [CrossRef]
13. Tong, P.; Wu, L.; Yanchen, A.; Su, R.; Wu, Y. A Novel Eddy Current Sensor for Displacement Measurement with High Accuracy and Long Range. *IEEE Sens. J.* **2023**, *23*, 12066–12075. [CrossRef]
14. Krupa, A.; Lackowski, M.; Jaworek, A. Capacitance sensor for measuring void fraction in small channels. *Measurement* **2021**, *175*, 109046. [CrossRef]
15. Beverte, I.; Cabulis, U.; Gaidukovs, S. Polytetrafluoroethylene Films in Rigid Polyurethane Foams' Dielectric Permittivity Measurements with a One-Side Access Capacitive Sensor. *Polymers* **2021**, *13*, 1173. [CrossRef] [PubMed]
16. Li, X.N.; Wang, R.; Du, H.M.; Lu, Y.Y. Three-dimensional micro-displacement measurement method based on capacitance-grating sensor. *Measurement* **2022**, *187*, 9. [CrossRef]
17. Ortlepp, I.; Zöllner, J.-P.; Rangelow, I.W.; Manske, E. Heterodyne Standing-Wave Interferometer with Improved Phase Stability. *Nanomanuf. Metrol.* **2021**, *4*, 190–199. [CrossRef]

18. TLS Collaboration; Aasi, J.; Abbott, B.; Abbott, R.; Abbott, T.; Abernathy, M.; Ackley, K.; Adams, C.; Adams, T.; Addesso, P. Advanced ligo. *Class. Quantum Gravity* **2015**, *32*, 074001. [CrossRef]
19. Li, X.; Cui, C. Grating interferometric precision nanometric measurement technology. *Opt. Precis. Eng.* **2024**, *32*, 2591–2611. [CrossRef]
20. Liu, W.Z.; Yu, Z.X.; Duan, F.J.; Hu, H.W.; Fu, X.; Bao, R.J. Robust five-degree-of-freedom measurement system with self-compensation and air turbulence protection. *Opt. Express* **2023**, *31*, 4652–4666. [CrossRef] [PubMed]
21. Zheng, F.; Feng, Q.; Zhang, B.; Li, J. A Method for Simultaneously Measuring 6DOF Geometric Motion Errors of Linear and Rotary Axes Using Lasers. *Sensors* **2019**, *19*, 1764. [CrossRef] [PubMed]
22. Hsieh, H.L.; Liang, A.J.; He, P.Y. Symmetrical double diffraction laser encoder. In Proceedings of the Optical Micro-and Nanometrology VII, Strasbourg, France, 22–26 April 2018; Volume 10678, pp. 160–166.
23. Gao, W. *Precision Nanometrology: Sensors and Measuring Systems for Nanomanufacturing*; Springer: London, UK, 2010.
24. Shimizu, Y. Laser Interference Lithography for Fabrication of Planar Scale Gratings for Optical Metrology. *Nanomanuf. Metrol.* **2021**, *4*, 3–27. [CrossRef]
25. Liu, Y.; Li, X.; Huang, J.; Wang, Z.; Zhao, X.; Zhao, B.; Jiang, L. High-Uniformity Submicron Gratings with Tunable Periods Fabricated through Femtosecond Laser-Assisted Molding Technology for Deformation Detection. *ACS Appl. Mater. Interfaces* **2022**, *14*, 16911–16919. [CrossRef] [PubMed]
26. Liang, J.J.; Wang, C.Y.; Lu, H.O.; Wang, X.H.; Ni, K.; Zhou, Q. Method for fabricating large-area gratings with a uniform duty cycle without a spatial beam modulator. *Opt. Express* **2021**, *29*, 27791–27806. [CrossRef] [PubMed]
27. Deng, X.; Tan, W.; Tang, Z.; Lin, Z.; Cheng, X.; Li, T. Scanning and Splicing Atom Lithography for Self-traceable Nanograting Fabrication. *Nanomanuf. Metrol.* **2022**, *5*, 179–187. [CrossRef]
28. Li, X.; Wang, H.; Ni, K.; Zhou, Q.; Mao, X.; Zeng, L.; Wang, X.; Xiao, X. Two-probe optical encoder for absolute positioning of precision stages by using an improved scale grating. *Opt. Express* **2016**, *24*, 21378–21391. [CrossRef] [PubMed]
29. Shi, Y.P.; Ni, K.; Li, X.H.; Zhou, Q.; Wang, X.H. Highly accurate, absolute optical encoder using a hybrid-positioning method. *Opt. Lett.* **2019**, *44*, 5258–5261. [CrossRef] [PubMed]
30. Ren, W.; Cui, J.; Tan, J. A Novel Enhanced Roll-Angle Measurement System Based on a Transmission Grating Autocollimator. *IEEE Access* **2019**, *7*, 120929–120936. [CrossRef]
31. Yusheng, J.; Jianjun, D.; Changsheng, L.; Yangpeng, L.; Xindong, L. Angle-error Separation and Self-calibration at Arbitrary Angular Positions for Circular Grating Encoders. *J. Mech. Eng.* **2026**, *62*, 25–36.
32. Gao, W.; Kim, S.W.; Bosse, H.; Haitjema, H.; Chen, Y.L.; Lu, X.D.; Knapp, W.; Weckenmann, A.; Estler, W.T.; Kunzmann, H. Measurement technologies for precision positioning. *CIRP Ann.* **2015**, *64*, 773–796. [CrossRef]
33. Gao, W. New encoder technologies. *J. Jpn. Soc. Precis. Eng.* **2016**, *82*, 773–777. [CrossRef]
34. Lynch, K.M.; Marchuk, N.; Elwin, M.L. Chapter 21-Sensors. In *Embedded Computing and Mechatronics with the PIC32 Microcontroller*; Newnes: Oxford, UK, 2016; pp. 317–340.
35. Hong, Y.; Sato, R.; Zhang, Z.; Matsukuma, H.; Manske, E.; Gao, W. Near-common-optical-path two-axis surface encoder with a three-layer gratings interference method. *Opt. Express* **2025**, *33*, 19951–19965. [CrossRef] [PubMed]
36. Yu, H.; Wan, Q.H.; Mu, Z.Y.; Du, Y.C.; Liang, L.H. Novel nano-scale absolute linear displacement measurement based on grating projection imaging. *Measurement* **2021**, *182*, 109738. [CrossRef]
37. Zhao, M.Q.; Yuan, Y.Y.; Luo, L.B.; Li, X.H. A Review: Absolute Linear Encoder Measurement Technology. *Sensors* **2025**, *25*, 5997. [CrossRef] [PubMed]
38. Yen, K.S.; Ratnam, M.M. Simultaneous measurement of 3-D displacement components from circular grating moiré fringes: An experimental approach. *Opt. Lasers Eng.* **2012**, *50*, 887–899. [CrossRef]
39. Zhao, C.; Wan, Q.; Lu, X.; Liang, L. Moir Fringe Signal Subdivision System of a Stained Code Disc of a Grating Displacement Sensor. *IEEE Sens. J.* **2022**, *22*, 8614–8621. [CrossRef]
40. HEIDENHAIN. Linear Encoders for Numerically Controlled Machine Tools. Available online: https://www.heidenhain.com.cn/fileadmin/pdf/zh_CN/Prospekte/PR_Linear_Encoders_for_Numerically_Controlled_Machine_Tools_ID571470_zh.pdf (accessed on 19 April 2026).
41. Lv, B.; Li, S.; Liu, J. Harmonic Suppression Method for Optical Encoder Based on Photosensitive Unit Parameter Optimization. *Optics* **2025**, *6*, 62. [CrossRef]
42. Yang, F.; Lu, X.; Kilikevicius, A.; Gurauskis, D. Methods for Reducing Subdivision Error within One Signal Period of Single-Field Scanning Absolute Linear Encoder. *Sensors* **2023**, *23*, 865. [CrossRef] [PubMed]
43. RENISHAW. TONiC™ Incremental Encoder Series. Available online: https://www.renishaw.com.cn/zh/tonic-optical-incremental-encoder-series--37824 (accessed on 19 April 2026).
44. Sina Finance. Have You Ever Used an Absolute Encoder? It Is Definitely the Most Precise Measurement Method, Without a Doubt. Available online: https://t.cj.sina.com.cn/articles/view/6258125218/1750369a200100fd40 (accessed on 19 April 2026).

45. HEIDENHAIN. Exposed Linear Encoders. Available online: https://www.heidenhain.com.cn/fileadmin/pdf/en/01_Products/Prospekte/PR_Exposed_Linear_Encoders_ID208960_en.pdf (accessed on 19 April 2026).
46. HEIDENHAIN. LIC 2100 Series. Available online: https://www.heidenhain.com/products/encoders/linear-encoders/exposed/lic-2100 (accessed on 19 April 2026).
47. RENISHAW. RESOLUTE™ True Absolute Optical Encoder. Available online: https://www.renishaw.com.cn/zh/safety-first-the-position-determination-and-checking-algorithms-of-the-resolute-true-absolute-optical-encoder--47195 (accessed on 19 April 2026).
48. Wang, S.; Luo, L.; Li, X. Design and parameter optimization of zero position code considering diffraction based on deep learning generative adversarial networks. *Nanomanuf. Metrol.* **2024**, *7*, 2. [CrossRef]
49. Zhang, M.; Lu, C.; Liu, W.; Liu, X.; Zhao, Q. Integrated Micro Sensor Based on Grating Interferometer: A Review. *IEEE Sens. J.* **2024**, *25*, 2073–2089. [CrossRef]
50. Huang, G.Y.; Cui, C.; Lei, X.Y.; Li, Q.X.; Yan, S.H.; Li, X.H.; Wang, G.C. A Review of Optical Interferometry for High-Precision Length Measurement. *Micromachines* **2025**, *16*, 6. [CrossRef] [PubMed]
51. Wang, G.; Gao, L.; Huang, G.; Lei, X.; Cui, C.; Wang, S.; Yang, M.; Zhu, J.; Yan, S.; Li, X. A Wavelength-Stabilized and Quasi-Common-Path Heterodyne Grating Interferometer with Sub-Nanometer Precision. *IEEE Trans. Instrum. Meas.* **2024**, *73*, 7002509. [CrossRef]
52. Lv, Q.; Li, W.; Bayanheshig; Bai, Y.; Liu, Z.; Wang, W. Interferometric precision displacement measurement system based on diffraction grating. *Chin. Opt.* **2017**, *10*, 39–50. [CrossRef]
53. Yu, H.Y.; Chen, X.L.; Liu, C.J.; Cai, G.G.; Wang, W.D. A survey on the grating based optical position encoder. *Opt. Laser Technol.* **2021**, *143*, 107352. [CrossRef]
54. Zhang, Z.; Zhao, G.; Ban, Y.; Wang, X.; Lei, B.; Wang, L.; Chen, B.; Gao, F.; Jiang, X.; Liu, H. Achieving high-fold optical subdivision of a blazed grating interferometer through near-Littrow incidence. *IEEE Trans. Instrum. Meas.* **2025**, *74*, 7010910. [CrossRef]
55. Ye, G.Y.; Liu, H.; Lei, B.; Niu, D.; Xing, H.W.; Wei, P.P.; Lu, B.H.; Liu, H.Z. Optimal design of a reflective diffraction grating scale with sine-trapezoidal groove for interferential optical encoders. *Opt. Lasers Eng.* **2020**, *134*, 106196. [CrossRef]
56. Zhao, G.; Ye, G.; Liu, H.; Lei, B.; Li, X.; Han, W.; Liu, H. Electronic Interpolation Interface Based on Linear Subdivision Method for Sinusoidal Optical Encoders. *IEEE Sens. J.* **2019**, *20*, 3646–3654. [CrossRef]
57. Ye, G.; Liu, H.; Wang, Y.; Lei, B.; Shi, Y.; Yin, L.; Lu, B. Ratiometric-Linearization-Based High-Precision Electronic Interpolator for Sinusoidal Optical Encoders. *IEEE Trans. Ind. Electron.* **2018**, *65*, 8224–8231. [CrossRef]
58. Ban, Y.W.; Zhao, G.B.; Zhang, Z.H.; Chen, B.D.; Lu, B.H.; Liu, H.Z. High-factor interpolation method based on space-time modulation and a Kalman filter for optical encoders. *Opt. Express* **2024**, *32*, 1914–1925. [CrossRef] [PubMed]
59. Niu, D.; Wang, X.H.; Li, T.; Su, J.Y.; Chen, B.D.; Ren, S.P.; Li, G.J.; Jiang, W.T.; Shi, Y.S.; Yin, L.; et al. High-order diffraction gratings with an isosceles triangle profile for a nano-precision linear optical encoder. *Opt. Lett.* **2025**, *50*, 7187–7190. [CrossRef] [PubMed]
60. Zhou, T.; Masui, S.; Michihata, M.; Takahashi, S. Ultra-High-Resolution Linear Scale Using Circular Optical System-Design of an Optical System for Enhanced Subdivision. In *Proceedings of the 2025 30th Microoptics Conference (MOC)*; IEEE: New York, NY, USA, 2025; pp. 1–2.
61. Zhou, W.Y.; Liu, Z.W.; Sun, Y.J.; Teng, H.R.; Wang, W.C.; Bayanheshig; Li, W.H. Bidirectional Littrow double grating interferometry for quadruple optical interpolation. *Opt. Laser Technol.* **2024**, *175*, 11. [CrossRef]
62. Zhang, Z.H.; Niu, D.; Zhao, G.B.; Ban, Y.W.; Wang, X.H.; Wei, P.; Jiang, W.T.; Chen, J.J.; Liu, H.Z. Improving the optical subdivision ability of a grating interferometer via double-row reverse blazed gratings. *Opt. Lasers Eng.* **2023**, *168*, 10. [CrossRef]
63. Yang, F.; Zhang, M.; Zhu, Y.; Ye, W.; Wang, L.; Xia, Y. Two Degree-of-Freedom Fiber-Coupled Heterodyne Grating Interferometer with Milli-Radian Operating Range of Rotation. *Sensors* **2019**, *19*, 3219. [CrossRef] [PubMed]
64. HEIDENHAIN. LIP 382 Incremental Exposed Linear Encoder for High Accuracy. Available online: https://www.heidenhain.com/service-support/infobase/607220-01 (accessed on 19 April 2026).
65. MAGNESCALE. Laserscale. Available online: https://www.magnescale.com/en/product/catalog/LS-EA02(01)'C_C.2503.CB.300.pdf (accessed on 19 April 2026).
66. Niiya, M. Technologies of self calibrated 2D encoder scale. *J. Jpn. Soc. Precis. Eng.* **2016**, *82*, 788–791. [CrossRef]
67. Fan, K.-C.; Chen, M.-J.; Huang, W. A six-degree-of-freedom measurement system for the motion accuracy of linear stages. *Int. J. Mach. Tools Manuf.* **1998**, *38*, 155–164. [CrossRef]
68. Cui, C.; Gao, L.; Zhao, P.; Yang, M.; Liu, L.; Ma, Y.; Huang, G.; Wang, S.; Luo, L.; Li, X. Towards multi-dimensional atomic-level measurement: Integrated heterodyne grating interferometer with zero dead-zone. *Light Adv. Manuf.* **2025**, *6*, 319–332. [CrossRef]
69. Hong, Y.; Sato, R.; Shimizu, Y.; Matsukuma, H.; Gao, W. A New Optical Configuration for the Surface Encoder with an Expanded Z-Directional Measuring Range. *Sensors* **2022**, *22*, 3010. [CrossRef] [PubMed]
70. Wang, S.T.; Luo, L.B.; Zhu, J.H.; Shi, N.N.; Li, X.H. An Ultra-Precision Absolute-Type Multi-Degree-of-Freedom Grating Encoder. *Sensors* **2022**, *22*, 9047. [CrossRef] [PubMed]

71. Shimizu, Y.; Lim, H.; Tashiro, N.; Kitazume, T. Development of an optical linear encoder with a function of calibrating scale pitch deviation. *CIRP Ann.* **2026**, *75*, 643–647. [CrossRef]
72. Hsieh, H.-L.; Cai, S.-Y. Development of a dual heterodyne grating interferometer for four degree-of-freedom displacement and angular displacement measurements. *Opt. Laser Technol.* **2025**, *193*, 114314. [CrossRef]
73. Gao, W.; Dejima, S.; Kiyono, S. A dual-mode surface encoder for position measurement. *Sens. Actuators A Phys.* **2005**, *117*, 95–102. [CrossRef]
74. Ban, Y.; Zhao, G.; Liu, H.; Zhang, Z.; Chen, B.; Lu, B.; Liu, H. Two-dimensional grating interferometer with nanometer accuracy. *AIP Adv.* **2023**, *13*, 125125. [CrossRef]
75. Chang, D.; Yin, Z.Q.; Sun, Y.K.; Hu, P.C.; Tan, J.B.; Fan, Z.G. Spatially Separated Heterodyne Grating Interferometer for In-Plane and Out-of-Plane Displacement Measurements. *Photonics* **2022**, *9*, 830. [CrossRef]
76. Yin, Y.F.; Liu, Z.W.; Jiang, S.; Wang, W.; Yu, H.Z.; Jiri, G.; Hao, Q.; Li, W.H. High-precision 2D grating displacement measurement system based on double-spatial heterodyne optical path interleaving. *Opt. Lasers Eng.* **2022**, *158*, 7. [CrossRef]
77. Wang, S.; Liao, B.; Shi, N.; Li, X. A Compact and High-Precision Three-Degree-of-Freedom Grating Encoder Based on a Quadrangular Frustum Pyramid Prism. *Sensors* **2023**, *23*, 4022. [CrossRef] [PubMed]
78. Zhu, J.; Wang, G.; Wang, S.; Li, X. A Reflective-Type Heterodyne Grating Interferometer for Three-Degree-of-Freedom Sub-nanometer Measurement. *IEEE Trans. Instrum. Meas.* **2022**, *71*, 7007509. [CrossRef]
79. Zhou, S.Y.; Le, V.; Xiong, S.L.; Yang, Y.T.; Ni, K.; Zhou, Q.; Wu, G.H. Dual-comb spectroscopy resolved three-degree-of-freedom sensing. *Photonics Res.* **2021**, *9*, 243–251. [CrossRef]
80. Zhu, M.J.; Wang, G.; Xue, G.; Zhou, Q.; Li, X. Heterodyne three-degree-of-freedom grating interferometer for ultra-precision positioning of lithography machine. In *Proceedings of the 2021 International Conference on Optical Instruments and Technology: Optoelectronic Measurement Technology and Systems*; SPIE: California, CA, USA, 2021; p. 21.
81. Gao, Z.Y.; Hu, J.C.; Zhu, Y.; Duan, G.H. A new 6-degree-of-freedom measurement method of X-Y stages based on additional information. *Precis. Eng.-J. Int. Soc. Precis. Eng. Nanotechnol.* **2013**, *37*, 606–620. [CrossRef]
82. Lei, W.T.; Chen, C.W. A high accuracy six-dimensional motion measuring device: Design and accuracy evaluation. *Mech. Mach. Theory* **2024**, *191*, 19. [CrossRef]
83. Cui, C.; Yang, M.; Liu, L.; Zhao, P.; Gao, L.; Li, X. A quasi-common-path heterodyne grating interferometer for six-degree-of-freedom measurement. In *Proceedings of the Optical Metrology and Inspection for Industrial Applications XI*; SPIE: California, CA, USA, 2024; pp. 115–125.
84. Tamiya, H.; Taniguchi, K.; Yamazaki, K.; Aoyama, H. Detection principle and verification of non-contact displacement meter with pico-meter resolution. *J. Adv. Mech. Des. Syst. Manuf.* **2018**, *12*, JAMDSM0107. [CrossRef]
85. Tamiya, H. Development of High-Precision Three-Dimensional Encoder Based on Stabilized Grating Interference Method. Doctoral Thesis, Keio University, Minato City, Tokyo, 2021.
86. Tamiya, H.; Mitera, Y.; Taniguchi, K.; Aoyama, H.; Yamazaki, K. Development of a three-dimensional encoder for highly accurate positioning. *J. Jpn. Soc. Precis. Eng.* **2018**, *85*, 891–895. [CrossRef]
87. HEIDENHAIN. KGM 282 Grid Encoder. Available online: https://www.heidenhain.com/service-support/infobase/1313025-01 (accessed on 19 April 2026).
88. Xia, H. Research on Precise 2-D Plane Grating Measurement System and Key Technology. Doctoral Thesis, Hefei University of Technology, Hefei, China, 2006.
89. Ye, W.; Zhang, M.; Zhu, Y.; Wang, L.; Hu, J.; Li, X.; Hu, C. Ultraprecision Real-Time Displacements Calculation Algorithm for the Grating Interferometer System. *Sensors* **2019**, *19*, 2409. [CrossRef] [PubMed]
90. Li, X.H.; Gao, W.; Muto, H.S.; Shimizu, Y.; Ito, S.; Dian, S. A six-degree-of-freedom surface encoder for precision positioning of a planar motion stage. *Precis. Eng.-J. Int. Soc. Precis. Eng. Nanotechnol.* **2013**, *37*, 771–781. [CrossRef]
91. Gao, W.; Kimura, A. A Three-axis Displacement Sensor with Nanometric Resolution. *CIRP Ann.* **2007**, *56*, 529–532. [CrossRef]
92. Gao, W.; Saito, Y.; Muto, H.; Arai, Y.; Shimizu, Y. A three-axis autocollimator for detection of angular error motions of a precision stage. *CIRP Ann.* **2011**, *60*, 515–518. [CrossRef]
93. Sawabe, M.; Maeda, F.; Yamaryo, Y.; Simomura, T.; Saruki, Y.; Kubo, T.; Sakai, H.; Aoyagi, S. A new vacuum interferometric comparator for calibrating the fine linear encoders and scales. *Precis. Eng.* **2004**, *28*, 320–328. [CrossRef]
94. Gao, W.; Kimura, A. A fast evaluation method for pitch deviation and out-of-flatness of a planar scale grating. *CIRP Ann.* **2010**, *59*, 505–508. [CrossRef]
95. Chen, X.; Shimizu, Y.; Xiong, X.; Chen, Y.-l.; Gao, W. Self-calibration of Fizeau interferometer and planar scale gratings in Littrow setup. *Opt. Express* **2017**, *25*, 21567–21582. [CrossRef] [PubMed]
96. Xiong, X.; Shimizu, Y.; Chen, X.; Matsukuma, H.; Gao, W. Uncertainty Evaluation for Measurements of Pitch Deviation and Out-of-Flatness of Planar Scale Gratings by a Fizeau Interferometer in Littrow Configuration. *Appl. Sci.* **2018**, *8*, 2539. [CrossRef]
97. Xiong, X.; Matsukuma, H.; Shimizu, Y.; Gao, W. Evaluation of the pitch deviation of a linear scale based on a self-calibration method with a Fizeau interferometer. *Meas. Sci. Technol.* **2020**, *31*, 094002. [CrossRef]

98. Xiong, X.; Shimizu, Y.; Matsukuma, H.; Gao, W. A Self-Calibration Stitching Method for Pitch Deviation Evaluation of a Long-Range Linear Scale by Using a Fizeau Interferometer. *Sensors* **2021**, *21*, 7412. [CrossRef] [PubMed]
99. Murphy, P.; Forbes, G.; Fleig, J.; Dumas, P.; Tricard, M. Stitching interferometry: A flexible solution for surface metrology. *Opt. Photonics News* **2003**, *14*, 38–43. [CrossRef]
100. Wang, H.; Wang, J.; Chen, B.; Xiao, P.; Chen, X.; Cai, N.; Ling, B.W.-K. Absolute optical imaging position encoder. *Measurement* **2015**, *67*, 42–50. [CrossRef]
101. Shimizu, Y.; Ishizuka, R.; Mano, K.; Kanda, Y.; Matsukuma, H.; Gao, W. An absolute surface encoder with a planar scale grating of variable periods. *Precis. Eng.* **2021**, *67*, 36–47. [CrossRef]
102. Xiong, X.; Quan, L.; Shimizu, Y.; Matsukuma, H.; Gao, W. Self-calibration of a variable-line-spacing grating for an absolute optical encoder with a Fizeau interferometer. *Meas. Sci. Technol.* **2021**, *32*, 064005. [CrossRef]
103. Xiong, X.; Yin, C.; Quan, L.; Sato, R.; Matsukuma, H.; Shimizu, Y.; Tamiya, H.; Gao, W. Self-Calibration of a Large-Scale Variable-Line-Spacing Grating for an Absolute Optical Encoder by Differencing Spatially Shifted Phase Maps from a Fizeau Interferometer. *Sensors* **2022**, *22*, 9348. [CrossRef] [PubMed]
104. Yin, C.; Xiong, X.; Sato, R.; Matsukuma, H.; Tamiya, H.; Gao, W. Conjugate differential self-calibration of a large-scale two-dimensional variable-line-spacing grating for an absolute optical encoder using a Fizeau phase-shifting interferometer. *Meas. Sci. Technol.* **2025**, *36*, 075023. [CrossRef]

Disclaimer/Publisher's Note: The statements, opinions and data contained in all publications are solely those of the individual author(s) and contributor(s) and not of MDPI and/or the editor(s). MDPI and/or the editor(s) disclaim responsibility for any injury to people or property resulting from any ideas, methods, instructions or products referred to in the content.